AD-A050 969 TDR INC LOS ANGELES CA F/G 20/14
NUMERICAL INVESTIGATION OF PLANE WAVE PULSE SCATTERING BY DIELE--ETC(U).
OCT 77 A D VARVATSIS, S G SIEGEL, M I SANCER AFOSR-76-3010
AFOSR-TR-78-0209 NL

UNCLASSIFIED

1 OF 2
ADA
050969

SECURITY CLASSIFICATION OF THIS PAGE (When Data Entered)

(18) (19) **REPORT DOCUMENTATION PAGE**

READ INSTRUCTIONS BEFORE COMPLETING FORM

1. REPORT NUMBER: AFOSR-TR-78-0209	2. GOVT ACCESSION NO. (2)
3. RECIPIENT'S CATALOG NUMBER	
4. TITLE (and Subtitle): NUMERICAL INVESTIGATION OF PLANE WAVE PULSE SCATTERING BY DIELECTRIC OBSTACLES/ DETAILED RESULTS FOR A DIELECTRIC SLAB MODEL OF THE ATLAS I TRESTLE PLATFORM.	5. TYPE OF REPORT & PERIOD COVERED: (9) Final rept.
	6. PERFORMING ORG. REPORT NUMBER
7. AUTHOR(s): (10) A. D./Varvatsis, S. G./Siegel, M. I./Sancer	8. CONTRACT OR GRANT NUMBER(s): (15) AFOSR-76-3010
9. PERFORMING ORGANIZATION NAME AND ADDRESS: TDR, Inc., Los Angeles, CA 90049	10. PROGRAM ELEMENT, PROJECT, TASK AREA & WORK UNIT NUMBERS: (16) 9751V05, 61102F (17) 05
11. CONTROLLING OFFICE NAME AND ADDRESS: AFOSR/NP, Bolling AFB, Bldg.#410, Wash DC 20332	12. REPORT DATE: (11) Oct 77 (12)
	13. NUMBER OF PAGES: 95 (97p.)
14. MONITORING AGENCY NAME & ADDRESS (if different from Controlling Office)	15. SECURITY CLASS. (of this report): Unclassified
	15a. DECLASSIFICATION/DOWNGRADING SCHEDULE

16. DISTRIBUTION STATEMENT (of this Report)

Approved for public release; distribution unlimited.

17. DISTRIBUTION STATEMENT (of the abstract entered in Block 20, if different from Report)

18. SUPPLEMENTARY NOTES

19. KEY WORDS (Continue on reverse side if necessary and identify by block number)

20. ABSTRACT (Continue on reverse side if necessary and identify by block number)

A system of time dependent integral equations are derived and then are analytically demonstrated to be capable of treating scattering by a dielectric interface. A finite difference method is demonstrated to be capable of determining the fields scattered by an obstacle having an edge, by comparing a numerical solution to a canonical solution for scattering by a perfectly conducting wedge. Both methods are applied to the dielectric platform which has both a dielectric interface as well as an edge. The results obtained are in close

DD FORM 1 JAN 73 1473 EDITION OF 1 NOV 65 IS OBSOLETE

UNCLASSIFIED

SECURITY CLASSIFICATION OF THIS PAGE (When Data Entered)

392 622

agreement and ~~we choose~~ chosen to generate production data for ATLAS I related parameters by employing the finite difference method; however, this should not be taken as an endorsement that this method is always preferable. As part of the investigation ~~we identify~~ are identified problems for which either method would be preferred. Finally, ~~we present~~ are presented time dependent plots of the electric field at points in the working volume that show the amount of distortion caused by the platform.

TDR, INC.
Los Angeles, California 90049

NUMERICAL INVESTIGATION OF PLANE WAVE PULSE SCATTERING BY DIELECTRIC OBSTACLES/DETAILED RESULTS FOR A DIELECTRIC SLAB MODEL OF THE ATLAS I TRESTLE PLATFORM

OCTOBER 1977

A. D. Varvatsis
S. G. Siegel
M. I. Sancer

ABSTRACT

A system of time dependent integral equations are derived and then are analytically demonstrated to be capable of treating scattering by a dielectric interface. A finite difference method is demonstrated to be capable of determining the fields scattered by an obstacle having an edge, by comparing a numerical solution to a canonical solution for scattering by a perfectly conducting wedge. Both methods are applied to the dielectric platform model which has both a dielectric interface as well as an edge. The results obtained are in close agreement and we choose to generate production data for ATLAS I related parameters by employing the finite difference method; however, this should not be taken as an endorsement that this method is always preferable. As part of the investigation we identify problems for which either method would be preferred. Finally, we present time dependent plots of the electric field at points in the working volume that show the amount of distortion caused by the platform.

CONTENTS

ILLUSTRATIONS

ACKNOWLEDGMENT OF GOVERNMENT RIGHTS AND SPONSORSHIP

Research sponsored by the Air Force Weapons Laboratory, under Grant No. AFOSR-76-3010. The United States Government is authorized to reproduce and distribute reprints for Governmental purposes notwithstanding any copyright notation hereon.

SECTION I

INTRODUCTION AND SUMMARY

The primary issue that pervaded this investigation was the question of how to achieve confidence in the numerical data that would be generated. The approach used was to compare the results obtained by two dissimilar calculational procedures after each was demonstrated to be capable of yielding results known to be valid for separate canonical problems. The two approaches are a coupled system of time dependent integral equations and an appropriate finite difference method.

The concern about the validity of the results is due to the fact that the plate model of the ATLAS I trestle platform requires the proper numerical treatment of a dielectric interface as well as an edge. The vast majority of numerical time dependent scattering calculations deal with scattering by a perfectly conducting obstacle and few of those studies focus on the effect of singularities caused in the solution due to an edge. We are not aware of any previous solution in the literature of the coupled system of integral equations that we derive, and numerically solve. The finite difference method that we employ has been previously used by Page and Peterson (ref. 1) for a dielectric interface; however, the procedure they employ at the interface is different from our procedure. This difference in the procedures does not appear to have serious consequence since numerical testing indicated that both procedures yield similar results for sufficiently small grid step size.

---

1. Page, W. E. and D. H. Peterson, A Numerical Method for Computing the Propagation of an Electromagnetic Pulse Guided Over a Material Interface, Sensor and Simulation Note 96, Air Force Weapons Laboratory, 1970.

The canonical problems used to test the system of integral equations are the problem of scattering by a dielectric half space and the problem of scattering by an infinite dielectric slab. For these problems, we analytically solve our system of integral equations and obtain the known solutions.

Our testing of the finite difference method was considerably more involved and a consequence of this testing has the potential for yielding significant side benefits. We utilize the known canonical solution for scattering of a plane wave step function by a perfectly conducting wedge. This solution was convolved with the function of time that we intended to choose for an incident plane wave pulse that would be convenient for us to treat by the finite difference method. The result of this convolution describes the scattering of a plane wave, having the desirable time dependence, by the perfectly conducting wedge. It is a simple matter to test that the results obtained by the convolution procedure are accurate to any prespecified number of significant figures. The test consists of increasing the number of points in the convolution integration procedure. We compared the results obtained by the finite difference method with the results of known accuracy obtained by the convolution approach and determined that the finite difference approach could also yield solutions to any prespecified number of significant figures by decreasing the finite difference grid step size.

The side benefit of this testing of the finite difference method was that we were able to show that the convolution solution and the finite difference solution were still in agreement when we let the wedge angle approach zero. This demonstrated that a particular finite difference method was capable of determining the field scattered by a particular perfectly conducting open surface (the semi-infinite half plane). This identifies an area of investigation that has

the potential to satisfy a long standing need in the area of EMP interaction and coupling. The question of whether an appropriate finite difference method is capable of determining the fields scattered by a nonplanar open surface merits a thorough investigation. This capability is necessary to quantify errors introduced by the many approximations currently employed to calculate the currents and voltages at the inputs of subsystems contained within metallic enclosures (missiles, aircraft, tanks, ships, etc.).

Returning to the question of confidence in the numerical data we present for the model of the ATLAS I trestle platform, we have explained how we concluded that the integral equation approach was capable of treating the dielectric interface problem and our finite difference method was capable of treating the edge problem. Our final test was to apply both methods to the dielectric plate, of finite extent and thickness, which has both an edge and a dielectric interface. The results obtained by the two methods were in agreement and we chose to use the finite difference method to generate the production runs that had parameters chosen to study the effect of TRESTLE's platform. For this particular problem, the finite difference method was chosen due to computer memory considerations; however, this should not be taken as an endorsement that this method is always preferable to use. As part our investigation we have identified problems for which either method would be preferred.

The results of our production runs show that, according to our simplified model of the platform, the fields in TRESTLE'S working volume are clearly distorted by the platform. This distortion occurs to the pulse shape as well as to its amplitude. As the observation point is chosen further in from the leading edge of the platform, the distortion persists for larger distances above the platform. Our present study is limited to a distance from the leading edge that corresponds

to 25 platform thicknesses. The observation distance is fundamentally limited by our two-dimensional modeling of a three-dimensional platform. The deeper in and higher up we choose to observe, the sooner we sense the effects of the sides of the platform that are not included in the two-dimensional model. Even with this limitation, our data is applicable for times longer than the time the incident field requires to achieve its maximum amplitude.

We view the amount of distortion exhibited by our model and calculations as demonstrating a need for further investigations, both theoretical and experimental, in order to assess and assist the threat relatability of tests that will be performed in ATLAS I. These investigations should include a more detailed model of the entire support structure as well as interactions with test objects and other portions of the simulator.

SECTION II

FORMULATION OF THE INTEGRAL EQUATION METHOD

In this section we derive the system of integral equations for the problem of scattering from a dielectric cylinder of infinite length and arbitrary cross section. The configuration of interest is depicted in figures 1a and 1b. The incident electromagnetic field is given by

$$\underline{E}^{inc} = E_o \, f(t - z'/c_o)\hat{e}_x$$

$$\underline{H}^{inc} = H_y^{inc} \, \hat{e}_y + H_z^{inc} \, \hat{e}_z$$

$$H_y^{inc} = \frac{E_o \cos \beta}{Z_o} f(t - z'/c_o), \quad H_z^{inc} = - \frac{E_o \sin \beta}{Z_o} f(t - z'/c)$$

$$z' = (z - z_o) \cos \beta + (y - y_o) \sin \beta \qquad (1)$$

where $\hat{e}_x$, $\hat{e}_y$, $\hat{e}_z$ are unit vectors, β is the angle defined in figures 1a and 1b, Z_o is the free-space characteristic impedance, c_o is the speed of light in free space and x_o, y_o, z_o are the coordinates of a point P_o on the surface of the cylinders, that is swept by the incident wavefront at $t = 0$ ($x_o = 0$).

The dielectric cylinder is homogeneous with a dielectric permittivity ϵ_i and a magnetic permeability μ_i equal to the vacuum permeability μ_o. Our problem is clearly two-dimensional, i.e., all the physical quantities of interest are independent of x. Under these circumstances one can show that the scattered electric field will only have an x-component whereas the scattered magnetic field will lie entirely in the yz plane. Maxwell's equations for the total field, incident plus scattered, are then reduced to

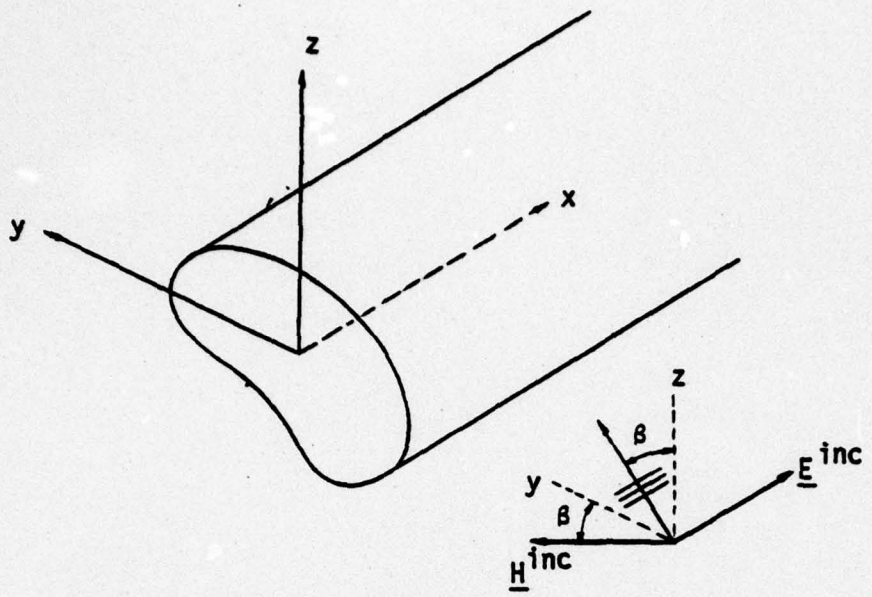

(a)

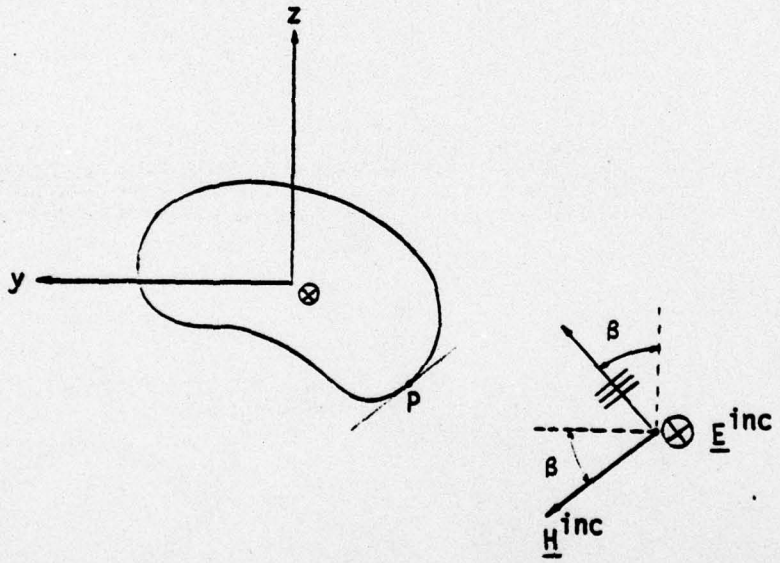

(b)

Figures 1. Three- and Two-Dimensional Geometries for the Scattering of an Electromagnetic Pulse from an Infinite Dielectric Cylinder

$$\frac{\partial E_x}{\partial y} = \mu_o \frac{\partial H_z}{\partial t}, \quad \frac{\partial E_x}{\partial z} = -\mu_o \frac{\partial H_y}{\partial t} \tag{2}$$

$$\varepsilon \frac{\partial E_x}{\partial t} = \frac{\partial H_z}{\partial y} - \frac{\partial H_z}{\partial z} - J_o(y,z,t) \tag{3}$$

where ε is equal to ε_o outside the body and equal to ε_i inside the body and $J_o(y,z,t)$ is the source of the incident field located far away from the scattering volume. (When $\varepsilon = \varepsilon_i$ the source term in Equation 3 should be set equal to zero.) The boundary conditions across the surface of the cylinder are: E_x and $\underline{H} \cdot \hat{s}$ continuous, i.e., total tangential electric and magnetic fields should be continuous (fig. 2). If the incident wavefront has a sharp front, i.e., the fields are nonzero there, then at $t = 0$ there is a discontinuity of the fields across the boundary. We will assume that $f(u)$ is a smooth function of u and define it more precisely as we treat our equations numerically in subsequent sections. For the derivation of the system of integral equations we need, as we shall see, continuity of E_x and $\partial E_x/\partial n$ where n is the outward normal on the surface of the cylinder. Continuity of $\partial E_x/\partial n$ is inferred by noting that (fig. 2)

$$\begin{aligned}
\frac{\partial E_x}{\partial n} &= \nabla_{yz} E_x \cdot \hat{n} = \frac{\partial E_x}{\partial y} \hat{n}_y + \frac{\partial E_x}{\partial z} \hat{n}_z \\
&= \frac{\partial E_x}{\partial y} (-\sin\theta) + \frac{\partial E_x}{\partial z} (\cos\theta) \\
&= \frac{\partial E_x}{\partial y} (-\hat{s}_z) - \frac{\partial E_x}{\partial z} (\hat{s}_y) \\
&= -\mu_o \frac{\partial}{\partial t} (H_z \hat{s}_z + H_y \hat{s}_y) = -\mu_o \frac{\partial}{\partial t} \underline{H} \cdot \hat{s}
\end{aligned} \tag{4}$$

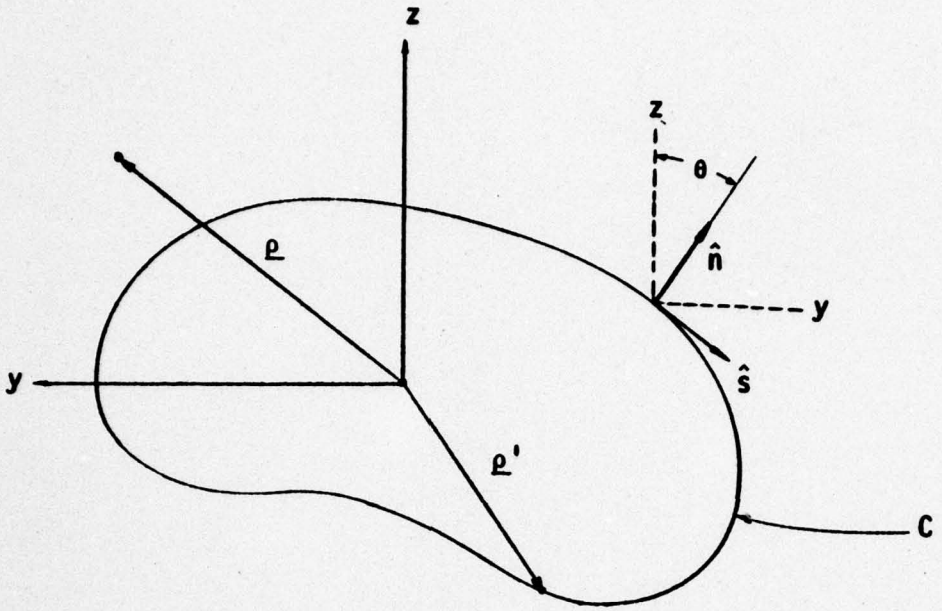

Figure 2. Geometry Depicting Certain Quantities Relevant to the Integral Equation Method for Solving the Scattering Problem

where the penultimate step employed equations 2. Since $\underline{H} \cdot \hat{s}$ is continuous across the boundary for all times we understand that so are $\partial/\partial t(\underline{H} \cdot \hat{s})$ and $\partial E_x/\partial n$. (We exclude pathological functions.)

Next we proceed to derive the system of integral equations that solves our two-dimensional scattering problem, i.e., it allows the calculation of the scattered fields inside and outside the dielectric body. We begin with the wave equation satisfied by E_x that can be derived by manipulating equations 2 and 3:

$$\left(\nabla^2_{y'z'} - \frac{1}{c^2}\frac{\partial^2}{\partial t'^2}\right)\Psi(\underline{\rho}',t') = F(\underline{\rho}',t') \qquad (5)$$

where $\underline{\rho}' = y'\hat{e}_y + z'\hat{e}_z$,

$\Psi \equiv E_x(\underline{\rho}',t')$ = total electric field

$c = c_o = (\mu_o\varepsilon_o)^{-1/2}$ outside the cylinder and

$c = c_i = (\mu_o\varepsilon_i)^{-1/2}$ inside the cylinder,

$F(\underline{\rho}',t') = \mu_o(\partial J_o/\partial t)$ outside the cylinder and

$F(\underline{\rho}',t') = 0$ inside the cylinder.

Next, we introduce the two-dimensional Green's function G satisfying

$$\left(\nabla^2_{y'z'} - \frac{1}{c^2}\frac{\partial^2}{\partial t'^2}\right)G(\underline{\rho}',\underline{\rho};\, t',t) = \delta(\underline{\rho}' - \underline{\rho})\,\delta(t' - t) \qquad (6)$$

$G(\underline{\rho}',\underline{\rho};\, t',t)$ is defined in an infinite free-space or an infinite dielectric medium depending on whether $c = c_o$ or $c = c_i$. The solution to equation 6 is

$$G(\underline{\rho}',\underline{\rho};\, t',t) = -\frac{c}{2\pi}\,\frac{U\left[\pm c(t'-t) - |\underline{\rho}'-\underline{\rho}|\right]}{\left[c^2(t'-t)^2 - (\underline{\rho}'-\underline{\rho})^2\right]^{1/2}} \tag{7}$$

where $U(x) = 1$ for $x > 0$ and $U(x) = 0$ for $x < 0$. The plus sign in equation 7 corresponds to the retarded solution, i.e., an observer at $\underline{\rho}'$ senses at t' a disturbance caused by a source at $\underline{\rho}$ fired at the retarded time $t = t' - |\underline{\rho}' - \underline{\rho}|/c$. The minus sign in equation 7 corresponds to the advanced solution, i.e., an observer at $\underline{\rho}'$ senses at t' a disturbance caused by a source at $\underline{\rho}$ fired at the advanced time $t = t' + |\underline{\rho}' - \underline{\rho}|/c$. This solution violates causality. Notice, however, that if we switch the observation and source space-time points the advanced solution of equation 7 becomes the retarded solution for the problem of a disturbance observed at $(\underline{\rho},t)$ and caused by a source at $\underline{\rho}'$ fired at $t' = t - |\underline{\rho}' - \underline{\rho}|/c$. This observation will be utilized later on when we derive our integral relationshps.

$$\int_{-\infty}^{\infty}\oint_C \left[\Psi(\underline{\rho}',t')\,\frac{\partial}{\partial n'}G_o(\underline{\rho}',\underline{\rho};\, t',t)\right.$$

$$\left. - G_o(\underline{\rho}',\underline{\rho};\, t',t)\,\frac{\partial}{\partial n'}\Psi(\underline{\rho}',t')\right]\, ds'dt'$$

$$-\frac{1}{c^2}\int_{-\infty}^{\infty}\int_{S_\infty}\frac{\partial}{\partial t'}\left[G_o(\underline{\rho}',\underline{\rho};\, t',t)\,\frac{\partial}{\partial t'}\Psi(\underline{\rho}',t')\right.$$

$$\left. -\Psi(\underline{\rho}',t')\,\frac{\partial}{\partial t'}\,G_o(\underline{\rho}',\rho;\, t',t)\right] dA'dt' = \Psi^{inc}(\underline{\rho},t) - \Psi(\underline{\rho},t)$$

(8)

where C is the contour shown in figure 2, $\hat{n}'$ is the outward normal (fig. 2), S_∞ is the region bounded by the circle at infinity and C and Ψ^{inc} is the incident electric field.

The derivation of equation 8 assumes that the contour integral at infinity (resulting from Green's identity) has been set equal to zero. The reason is that Ψ and $\partial\Psi/\partial n'$ in the integrals can be replaced by the scattered fields (one can see this by applying equation 8 for $\Psi = \Psi^{inc}$) and, for any finite t' or $-\infty$, they are zero. Thus the integration in t' is over one instant only ($t' = +\infty$) and it can be shown to have zero contribution. The t'-integration in the second integral in equation 8 can be performed explicitly. At $t' = -\infty$ the scattered fields are zero throughout region S_∞ and at $t' = \infty$ have gone to zero smoothly to assure that the integral over S is zero. Thus equation 8 can be rewritten as

$$\Psi(\underline{\rho},t) = \Psi^{inc}(\underline{\rho},t) - \int_{-\infty}^{\infty} \oint_C \left[\Psi(\underline{\rho}',t') \frac{\partial}{\partial n'} G_o(\underline{\rho}',\underline{\rho};\, t',t) - G_o(\underline{\rho}',\underline{\rho};\, t',t) \frac{\partial}{\partial n'} \Psi(\underline{\rho}',t')\right] ds'dt'. \qquad (9)$$

As we can see from equation 9 the scattered field at $\underline{\rho}$ and t is due to contributions from points $\underline{\rho}'$ on the contour firing at t'. Thus t' must be less than t and if we recall equation 7 we understand that $G(\underline{\rho}',\underline{\rho};\, t',t)$ must be taken with the minus sign in front of $c(t' - t)$, i.e., it is the advanced solution of equation 6 with $c = c_o$.

For the region inside the contour C we can apply a similar procedure and arrive at the following equation

$$\Psi(\underline{\rho},t) = \int_{-\infty}^{\infty} \oint_C \Big[\Psi(\underline{\rho}',t)\ \frac{\partial}{\partial n'}\ G_i(\underline{\rho}',\underline{\rho};\ t',t)$$

$$- G_i(\underline{\rho}',\underline{\rho};\ t',t)\ \frac{\partial}{\partial n'}\ \Psi(\underline{\rho}',t')\Big]\ ds'dt' \qquad (10)$$

where C is the same contour as in equation 9, $\hat{n}'$ is the outward normal and the Green's function G_i is the <u>advanced</u> solution of equation 6 with $c = c_i$.

In order to obtain our system of integral equations we let the observation point $\underline{\rho}$ approach the contour C. If the contour C is smooth then the singularity due to $\partial G/\partial n'$ at $\underline{\rho}' = \rho$ results in a term $\pm(1/2)\Psi(\underline{\rho},t)$ (plus for the inside and minus for the outside) and equations 9 and 10 give

$$\frac{1}{2}\ \Psi_o(\underline{\rho},t) = \Psi^{inc}(\underline{\rho},t) - \int_{-\infty}^{\infty} \oint_C \left(\Psi_o\ \frac{\partial G_o}{\partial n'} - G_o\ \frac{\partial \Psi_o}{\partial n'}\right) ds'dt'$$

$$\frac{1}{2}\ \Psi_i(\underline{\rho},t) = \int_{-\infty}^{\infty} \oint_C \left(\Psi_i\ \frac{\partial G_i}{\partial n'} - G_i\ \frac{\partial \Psi_i}{\partial n'}\right) ds'dt' \qquad (11)$$

where we have used the subscripts "o" and "i" to denote the outside and inside of the cylinder respectively. One can show that a principal value integration over C (resulting from the limiting process $\underline{\rho} \to \underline{\rho}'$ from the outside) is not necessary because the kernel in the integral is not singular as $\underline{\rho}' \to \underline{\rho}$ when both $\underline{\rho}$ and $\underline{\rho}'$ lie on the contour. (A contour with sharp corners is discussed at the end of this section.)

If we recall the continuity of Ψ and $\partial\Psi/\partial n$ as we cross the boundary contour we understand that $\Psi_o = \Psi_i \equiv \Psi(\underline{\rho},t)$ and

$\partial\Psi_o/\partial n = \partial\Psi_i/\partial n \equiv \partial\Psi/\partial n$ where $\underline{\rho}$ is on the contour C. Thus equations 11 represent a system of integral equations which allow the determination of Ψ and $\partial\Psi/\partial n$ on the boundary contour C. Once these quantities are known one can employ equations 9 and 10 to determine Ψ outside the body and inside the body respectively. Then Maxwell's equations 2 allow the determination of $\underline{H}$ everywhere.

In order to cast our system of equations into a form amenable to numerical treatment we employ the explicit form of G given by equation 7 and manipulate the resulting integrals to eliminate the apparent singular behavior that results from the differentiation of G. We have,

$$\frac{\partial G}{\partial n'} = \nabla' G \cdot \hat{n}' = \frac{\partial G}{\partial R} \nabla_{\underline{\rho}'} R \cdot \hat{n}' = \frac{\partial G}{\partial R} \frac{\underline{\rho}' - \underline{\rho}}{R} \cdot \hat{n}' \qquad (12)$$

where $R = |\underline{\rho}' - \underline{\rho}|$

$$\frac{\partial G}{\partial R} = -\frac{c}{2\pi} \left\{ - \frac{\delta[c(t - t') - R]}{\left[c^2(t - t')^2 - R^2\right]^{1/2}} + \frac{R}{\left[c^2(t - t')^2 - R^2\right]^{3/2}} U[c(t - t') - R] \right\} \qquad (13)$$

If we combine equations 12 and 13 we can write

$$\int_{-\infty}^{\infty} \Psi \frac{\partial G}{\partial n'} dt' = + \frac{1}{2\pi} \left[\frac{\Psi(\underline{\rho}', t')}{\left[c^2(t - t')^2 - R^2\right]^{1/2}} \frac{(\underline{\rho}' - \underline{\rho}) \cdot \hat{n}'}{R} \right]_{t'=t-R/C} - \frac{c}{2\pi} \int_{-\infty}^{\infty} \frac{\Psi(\underline{\rho}', t')(\underline{\rho}' - \underline{\rho}) \cdot \hat{n}'}{\left[c^2(t - t')^2 - R^2\right]^{3/2}} U[c(t - t') - R] \, dt' \qquad (14)$$

Recalling that

$$\int \frac{dt'}{[c^2(t-t')^2 - R^2]^{3/2}} = \frac{t-t'}{R^2[c^2(t-t')^2 - R^2]^{1/2}}$$

we can rewrite the integral on the right-hand side of equation 14 as

$$-\frac{c}{2\pi}\int_{-\infty}^{\infty} \frac{\Psi(\underline{\rho}',t')(\underline{\rho}' - \underline{\rho}) \cdot \hat{n}'}{[c^2(t-t')^2 - R^2]^{3/2}} U[c(t-t') - R]\, dt'$$

$$= -\frac{c}{2\pi}\int_{-\infty}^{\infty} \Psi(\underline{\rho}',t')(\underline{\rho}' - \underline{\rho}) \cdot \hat{n}'\, U[c(t-t') - R] \frac{d}{dt'}$$

$$\left[\frac{t-t'}{R^2[c^2(t-t')^2 - R^2]^{1/2}}\right] dt'$$

$$= -\frac{c}{2\pi} \frac{(t-t')\,\Psi(\underline{\rho}',t')\,U[c(t-t') - R]\,(\underline{\rho}' - \underline{\rho}) \cdot \hat{n}'}{R^2[c^2(t-t')^2 - R^2]^{1/2}}\Bigg|_{-\infty}^{\infty}$$

$$+\frac{c}{2\pi}\int_{-\infty}^{\infty} \frac{(t-t')(\underline{\rho}' - \underline{\rho}) \cdot \hat{n}'}{R^2[c^2(t-t')^2 - R^2]^{1/2}} \left\{U[c(t-t') - R] \frac{\partial \Psi}{\partial t'}\right.$$

$$\left. - c\Psi\delta[c(t-t') - R]\right\} dt'$$

$$= -\frac{c}{2\pi}\int_{-\infty}^{\infty} \frac{(t'-t)(\underline{\rho}' - \underline{\rho}) \cdot \hat{n}'}{R^2[c^2(t-t')^2 - R^2]^{1/2}} U[c(t-t') - R] \frac{\partial \Psi}{\partial t'}\, dt'$$

$$-\frac{1}{2\pi}\left[\frac{\Psi(\underline{\rho}' - t')(\underline{\rho}' - \underline{\rho}) \cdot \hat{n}'}{R[c^2(t-t')^2 - R^2]^{1/2}}\right]_{t' = t - R/c} \qquad (15)$$

If we compare equation 14 to equation 15 we see that

$$\int_{-\infty}^{\infty} \Psi \frac{\partial G}{\partial n'} dt'' = - \frac{c}{2\pi} \int_{-\infty}^{\infty} \frac{(t' - t)(\underline{\rho}' - \underline{\rho}) \cdot \hat{n}'}{R^2 [c^2 (t - t')^2 - R^2]^{1/2}} \frac{\partial \Psi'}{\partial t'} dt' \tag{16}$$

If we now return to our system of equations 11, we can use equation 16 to rewrite them as

$$\frac{1}{2} \Psi(\underline{\rho}, t) = \Psi^{inc}(\underline{\rho}, t) + \frac{c_o}{2\pi} \int_{-\infty}^{\infty} \oint_C \left[\frac{(\underline{R} \cdot \hat{n}')(t' - t)}{R^2} \frac{\partial \Psi}{\partial t'} \right.$$

$$\left. - \frac{\partial \Psi}{\partial n'} \right] \frac{U[c_o(t - t') - R]}{\left[c_o^2 (t - t')^2 - R^2\right]^{1/2}} ds' dt'$$

$$\frac{1}{2} \Psi(\underline{\rho}, t) = - \frac{c_i}{2\pi} \int_{-\infty}^{\infty} \oint_C \left[\frac{(\underline{R} \cdot \hat{n}')(t' - t)}{R^2} \frac{\partial \Psi}{\partial t'} - \frac{\partial \Psi}{\partial n'} \right]$$

$$\frac{U[c_i(t - t') - R]}{\left[c_i^2 (t - t')^2 - R^2\right]^{1/2}} ds' dt' \tag{17}$$

where $\underline{R} = \underline{\rho}' - \underline{\rho}$, $R = |\underline{\rho} - \underline{\rho}'|$, $c_o = (\mu_o \varepsilon_o)^{-1/2}$, $c_i = (\mu_o \varepsilon_i)^{-1/2}$ and $\hat{n}'$ is the outward normal on C (fig. 2). The integrands in the above system of integral equations appear singular when $R = 0$ and/or $c(t - t') = R$. The $R = 0$ singularity is only apparent because it can be shown that $\underline{R} \cdot \hat{n}'$ behaves as R^{α} where $\alpha \geq 2$ when $R \to 0$. The $c(t - t') = R$ singularity

is integrable because of the two-dimensional integration. When $R = 0$ and $c(t - t') = R$ simultaneously, i.e., $R = 0$, $t = t'$, the factor $t - t'$ provides an extra zero and the $R = 0$ singularity is still only apparent.

So far we have restricted our discussion to smooth contours. In this report we are interested in the numerical solution for the problem of scattering of an electromagnetic pulse from an infinite dielectric cylinder of a rectangular cross section. Thus the behavior of equations 17 in the vicinity of sharp corners (edges) must be examined. When the observation point $\underline{\rho}$ does not lie at a corner, equations 17 are still true. This is so because it is well-known that Ψ is finite at the edge and $\partial\Psi/\partial n$ varies no faster than $s^{-1/2}$, where s is the distance from the edge; consequently the integrals involving $\partial\Psi/\partial n$ have an integrable singularity and are well behaved. When the observation point $\underline{\rho}$ is allowed to approach a corner, the factor that is extracted from the integral involving $\partial G/\partial n$ is equal to $\pm(\Omega/2\pi)\Psi$ rather than $\pm 1/2$ (Ω is the interior angle shown in fig. 3) and consequently when $\underline{\rho}$ is at a corner equations 11 and 17 have their left-hand sides equal to $(1 - \Omega/2\pi)\Psi_{o,i}$. Our numerical treatment for the pair of integral equations 17 will not allow $\underline{\rho}$ to lie at a corner because all the reference points are chosen at the midpoints of arc segments as we will explain in the next section. Thus the factor to be extracted is $\pm 1/2$ and equations 17 are valid for all observation points of interest.

Before we turn our attention to the next section we should mention that in appendices A and B the validity of equations 17 is tested analytically by solving two special problems whose solutions are known.

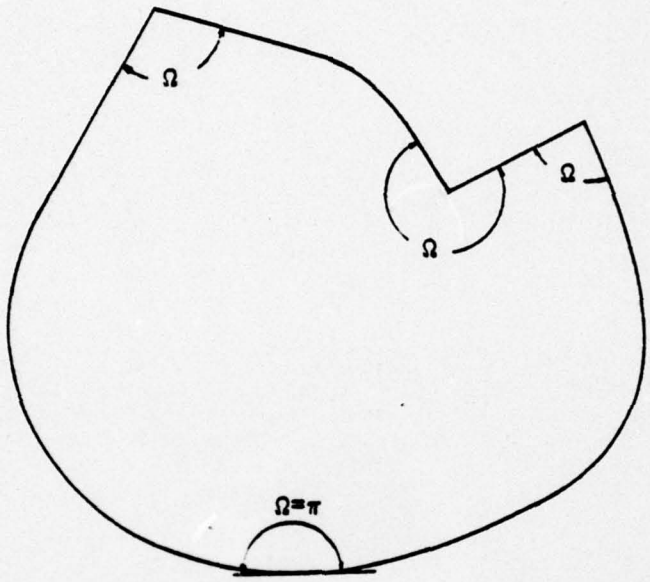

Figure 3. Geometry for the Definition of the Interior Angle Ω

SECTION III

NUMERICAL TREATMENT OF INTEGRAL EQUATIONS

In this section we present the procedure that allows us to numerically solve equations 17 for the problem of scattering of an electromagnetic wave from an infinite dielectric cylinder of a rectangular cross section (fig. 4) i.e., a rectangular slab. The incident wave is E-polarized in the x direction and propagates in the z direction. (Even though we focus our attention on the numerical solution for a <u>particular</u> cross section the method we employ is directly applicable to other cross sectional geometries.) In order to cast equations 17 into a system of algebraic equations which we can solve numerically, we partition each of the four sides of the rectangle in figure 4 into equal-sized intervals Δs and the midpoint of each line segment is chosen as the reference point for that interval. (Δs may vary from side to side.) In order to effect a similar partition for the t-integration we observe that the upper limit in equations 17 can be replaced by t since there can be no contribution to $\Psi(\underline{\rho},t)$ later than t. Assuming that the wavefront hits the front size of the rectangle at t = 0 we can replace the lower limit of the t-integrations by zero. If we set t = 0 in equations 17 we obtain $(1/2)\Psi_o(\underline{\rho},o) = \Psi^{inc}(\underline{\rho},o)$ and $\Psi_i(\underline{\rho},o) = 0$. There is no contradiction because the incident wave has a smooth wavefront and $\Psi^{inc}(\underline{\rho},o) = 0$ at all $\underline{\rho}$ on the contour. If the latest time of interest t is called T then we have a time interval (o,T) that can be partitioned into equal-sized intervals Δt.

The reference point for the j^{th} time interval, bounded by $t_{j-1} = (j - 1)\Delta t$ and $t_j = j\Delta t$, is t_j and not the midpoint $(j - 1/2)\Delta t$. The Cartesian product of the space and time partitions produces a lattice of zones. The <u>reference point for the i,j</u> zone is then $(i - 1/2)\Delta s$, $j\Delta t$, if for convenience all line segments are of equal size. Before we transform the pair of integral equations 17 into a system of

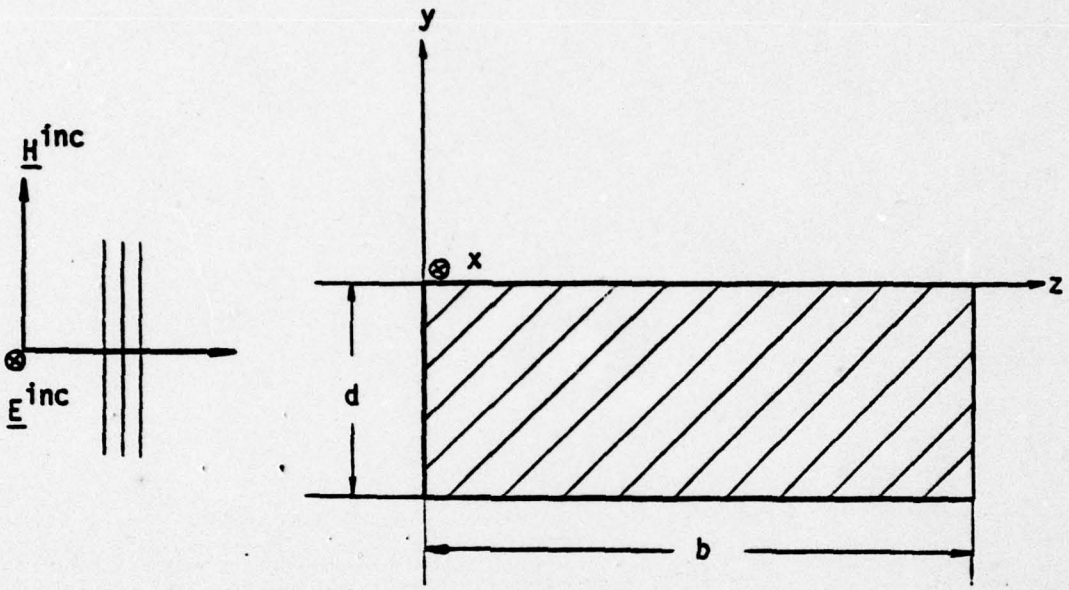

Figure 4. Geometry Depicting the Electromagnetic Pulse Incident on an Infinite Dielectric Cylinder of Rectangular Cross Section

algebraic equations which can be solved numerically we rewrite equations 17 in a more convenient form

$$\Psi(y,z,t) = S(y,z,t) - \int_o^t \oint_C [K_1(y,z,t;\, y',z',t')\Phi(y',z',t') + K_2(y,z,t;\, y',z',t')\dot{\Psi}(y',z',t')]\, ds'dt'$$

$$\Psi(y,z,t) = \int_o^t \oint_C [K_3(y,z,t;\, y',z',t')\Phi(y',z',t') + K_4(y,z,t;\, y',z',t')\dot{\Psi}(y',z',t')]\, ds'dt' \qquad (18)$$

where $\Phi \equiv \partial\Psi/\partial n'$, $\dot{\Psi} \equiv \partial\Psi/\partial t$, $S \equiv 2\Psi^{inc}$

$$K_1 = \frac{c_o}{\pi} \frac{U[c_o(t-t') - R]}{\left[c_o^2(t-t')^2 - R^2\right]^{1/2}}$$

$$K_2 = \frac{c_o}{\pi} \frac{(\underline{R} \cdot \hat{n}')(t-t')}{R^2} \frac{U[c_o(t-t') - R]}{\left[c_o^2(t-t')^2 - R^2\right]^{1/2}}$$

$$K_3 = K_1(c_o \to c_i) \qquad K_4 = K_2(c_o \to c_i). \qquad (19)$$

Our method of solving the system of equations 18 is to assume that $\dot{\Psi}$ and Φ vary so slowly in space and time that their values at a point defined by the midpoints of the arc segment and time interval forming a zone provide a good estimate for their values over the corresponding zone. The singular nature of the kernels forbids us from making the

same assumption about them. If we divide the circumference of the contour C into N segments we can rewrite equations 18 at $t = t_j$ as

$$\psi_i^j = S_i^j - \sum_{k=1}^{N} \sum_{\ell=1}^{j} \left[\phi_k^{\ell-1/2} \int_{A_{k\ell}} K_1 \, ds'dt' + \dot{\psi}_k^{\ell-1/2} \int_{A_{k\ell}} K_2 \, ds'dt' \right]$$

$$\psi_i^j = \sum_{k=1}^{N} \sum_{\ell=1}^{j} \left[\phi_k^{\ell-1/2} \int_{A_{k\ell}} K_3 \, ds'dt' + \dot{\psi}_k^{\ell-1/2} \int_{A_{k\ell}} K_4 \, ds'dt' \right] \quad (20)$$

where $F_{m_{th}}^n \equiv F(\underline{\rho}_m, n\Delta t)$, $\underline{\rho}_m$ is the radius vector to the midpoint of the m^{th} arc segment, $A_{k\ell}$ is the (k,ℓ) zone in the s,t space and $K_p \equiv K_p(\underline{\rho}_i, t_j; \underline{\rho}', t')(p = 1,2,3,4)$.

The time derivative is defined as

$$\dot{\psi}_k^{\ell-1/2} = (\psi_k^{\ell} - \psi_k^{\ell-1})/\Delta t$$

Thus $\dot{\psi}_k^{1/2} = (\psi_k^1 - \psi_k^0)/\Delta t = \psi_k^1/\Delta t$ since $\psi_k^0 = 0$.

At $j = 1$ equations 20 give

$$\psi_i^1 = S_i^1 - \sum_{k=1}^{N} \phi_k^{1/2} \int_{A_{k1}} K_1 \, ds'dt' + (\psi_k^1/\Delta t) \int_{A_{k1}} K_2 \, ds'dt'$$

$$\psi_i^1 = \sum_{k=1}^{N} \phi_k^{1/2} \int_{A_{k1}} K_3 \, ds'dt' + (\psi_k^1/\Delta t) \int_{A_{k1}} K_4 \, ds'dt'. \quad (21)$$

This is a system of 2N equations with 2N unknowns and can be solved to give Ψ_i^1, $\Phi_i^{1/2}$ (i=1,2,...,N) in terms of the known quantities S_i^1. If we write the system of equations 20 at j = 2, we again obtain a system of 2N equations for 2N unknowns Ψ_i^2, $\Phi_i^{3/2}$ in terms of the known quantities S_i^2, Ψ_i^1, $\Phi_1^{1/2}$ (i=1,2, ...,N). Thus we can march in time and solve for Ψ_i^j and $\Phi_i^{j-1/2}$ for any i and j in terms of the known quantities S_i^j, Ψ_i^ℓ, $\Phi_i^{\ell-1/2}$ (i=1,2,...,N; ℓ = 1,2,...,j-1). Once we obtain Ψ_i^j and $\Phi_i^{j-1/2}$ we can return to integral relationships 9 and 10 and calculate Ψ off the surface of the cylinder.

Notice that so far no restriction has been placed on the relative magnitude between Δt and $R = |\underline{\rho}' - \underline{\rho}|$. Integrals $\int_{A_{k\ell}} K_p \, ds'dt'$ in equation 20 represent the interaction between the various spatial segments and their importance depends on the relative magnitude of Δt and R (the distance between points) as we will explain shortly. To make this clear consider equations 21 written for j = 1. In this equation Ψ_i^1, i.e., Ψ evaluated at the midpoint of the i^{th} line segment and at $t = \Delta t$, depends on Φ and Ψ at the midpoints of all other line segments at $t = \Delta t$. A 2N x 2N matrix has to be inverted in order to evaluate Ψ_i^1. However, it is possible to choose Δt such that Ψ_i^1 and in general Ψ_i^j only depends on Ψ and Φ evaluated at the various midpoints at earlier times without inverting a 2N x 2N matrix, i.e., each pair of equations 20 will be solved for Ψ_i^j and $\Phi_i^{j-1/2}$ in terms of S_i^j, Ψ_i^ℓ $\Phi_i^{\ell-1/2}$ (ℓ=1,2,...,j-1) by inverting a 2 x 2 matrix. The restriction to be imposed on Δt is $\Delta t \leq \Delta s/2$ where Δs the size of line segments into which the sides of the rectangle have been partitioned. (We assume that all line segments are of equal size; if not, Δs is the smallest line segment.) The above restriction will now be illustrated. We proceed by writing equation 21 for i = 2, where the line segment i = 2 is depicted in figure 5.

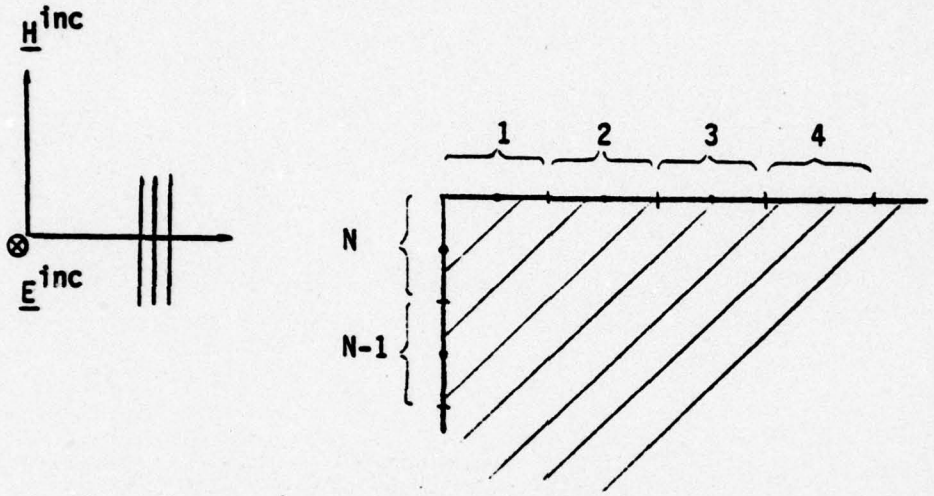

Figure 5. Partition of the Perimeter of the Rectangular Cross Section into N Equal-Sized Segments

$$\psi_2^1 = s_2^1 - \sum_{k=1}^{N} \left[\phi_k^{1/2} \int_{A_{k1}} K_1 \, ds'dt' + (\psi_k^1/\Delta t) \int_{A_{k1}} K_2 \, ds'dt' \right]$$

$$\psi_2^1 = \sum_{k=1}^{N} \left[\phi_k^{1/2} \int_{A_{k1}} K_3 \, ds'dt' + (\psi_k^1/\Delta t) \int_{A_{k1}} K_4 \, ds'dt' \right] \quad (22)$$

Let us consider in particular the interaction between line segments 1 and 2. This interaction is represented by the <u>influence coefficient</u> $\int_{A_{11}} K_p(\underline{\rho}_2, \Delta t; \underline{\rho}', t') \, ds'dt'$ (p=1,2,3,4). (Actually $K_2 = K_4 = 0$ if both the reference and integration points lie on the same side of the rectangle since $\underline{R} \cdot \hat{n} = 0$.) If we recall equations 19 we observe that K_p contains the step function U and the integration is to be performed over that portion of A_{11} that make U = 1, i.e., $c(t - t') - R \geq 0$ or $c(t - t') - |z - z'| \geq 0$. This last inequality defines a region of influence or a light "cone" in the ct',z' coordinate system (fig. 6). The exact location of this light "cone" depends on the values of z and t and in the present case $z = \Delta s/2$ and $t = \Delta t$. In figure 7 we have plotted zone A_{11} (defined by z' = 0, Δs and t = 0, Δt) for $c_o \Delta t = \Delta s/2$, Δs, $3\Delta s/2$ in a $c_o t', z'$ space. The case $c = c_i$ will be examined shortly. Notice that for $c_o \Delta t > \Delta s/2$ the influence coefficient $\int_{A_{11}} K_1 \, dz'dt'$ is nonzero, since the light "cone" intersects part of A_{11}, i.e., the line segment 1 influences line segment 2 during the time interval Δt and consequently ψ_2^1 in the first of equations 22 depends on $\phi_1^{1/2}$, i.e., on ϕ evaluated at a different point but at the same time (j = 1). However, if $c_o \Delta t \leq \Delta s/2$ then $\int_{A_{11}} K_1 \, dz'dt' = 0$ and also $\int_{A_{11}} K_3 \, dz'dt' = 0$ since $c_i \Delta t < c_o \Delta t$ and ψ_2^1 in equations 22 does not depend on $\phi_1^{1/2}$ (or ψ_1^1 since $K_2 = K_4 = 0$).

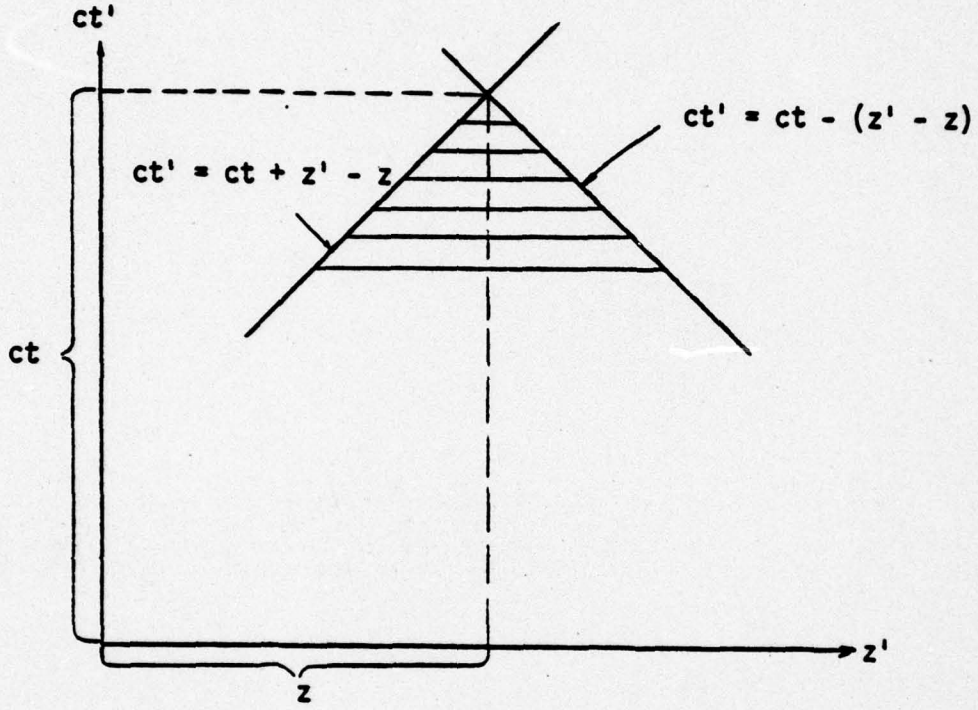

Figure 6. The Shaded Area Represents the Light "Cone" or Region of Influence for the Interaction Between Points Lying on the Same Side of the Rectangular Cross Section (Here the y=0 Side)

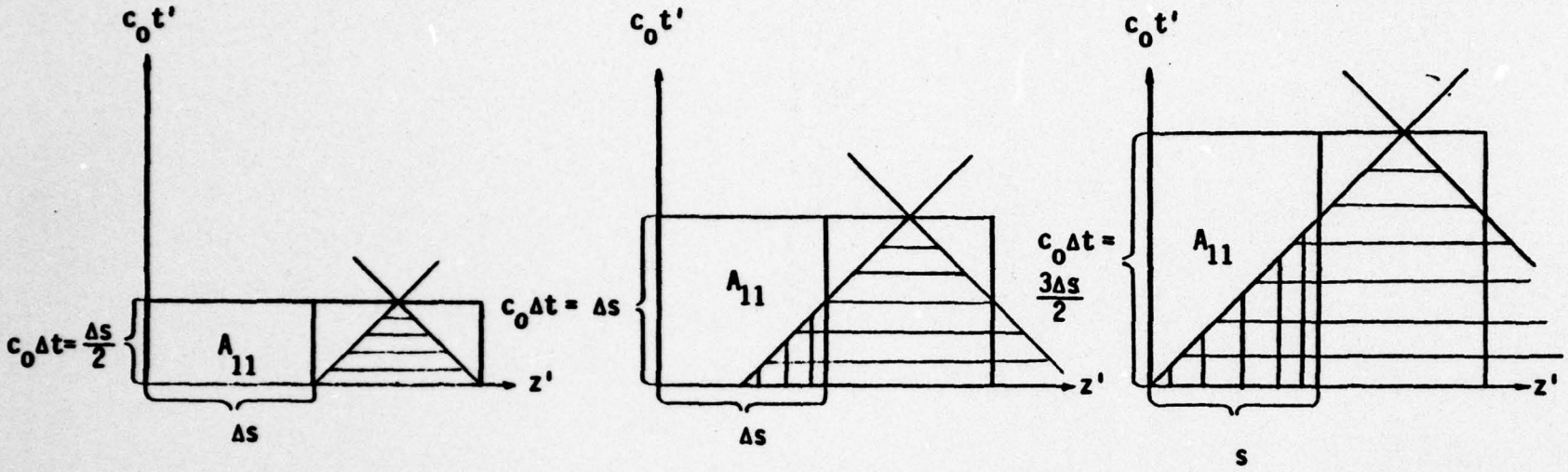

Figure 7. Diagrams Showing the Dependence of Influence Coefficients, for the Interaction of Line Segment 1 and Midpoint of Line Segment 2 (fig. 5), on the Temporal Step Size Δt

Next consider the influence coefficient between line segments 1 and N, i.e., line segments not lying on the same side of the rectangle (fig. 5) and write equation 21 for $i = N$. Again we examine the influence coefficients $\int_{A_{11}} K_p \, dz'dt'$. If we set $U = 1$, i.e., $c(t - t') - R \geq 0$ or $c(t - t') - (z'^2 + y^2)^{1/2} \geq 0$ we find that the region of influence or light "cone" is a branch of a hyperbola shown in figure 8. In figure 9 we have plotted zone A_{11} (defined by $z = 0$, Δs and $t = 0$, Δt) for $c_o \Delta t = \Delta s/2$, Δs, $3\Delta s/2$ in the $c_o t'$, z' space. (Notice that $y = -\Delta s/2$.) These plots exhibit similar features as those in figure 7, i.e., the integral over A_{11} is zero if $c_o \Delta t \leq \Delta s/2$. In general, the presence of U dictates that the influence coefficent will be zero if $t \leq t' + R/c$. When $t = \Delta t$ this inequality is satisfied for all t' $(0 \leq t' \leq \Delta t)$ if $\Delta t \leq R/c$. The smallest R is $\Delta s/2$, since the reference point is located at the middle of a line segment, i.e., $c\Delta t \leq \Delta s/2$. When $t = n\Delta t$ and $(n - 1)\Delta t \leq t' \leq n\Delta t$ we again obtain the same criterion. Bearing the previous discussion in mind, we can rewrite equations 21 as

$$\Psi_i^1 = S_i^1 - (K_1)_{i1} \, \Phi_i^{1/2}$$

$$\Psi_i^1 = (K_3)_{i1} \, \Phi_i^{1/2} \qquad \text{(21a)}$$

where $(K_p)_{k\ell} \equiv \int_{\Delta_{k\ell}} K_p \, ds'dt'$. Notice that all influence coefficients are zero except the self-terms $(K_1)_{i1}$ and $(K_3)_{i1}$. (The other two self-terms $(K_2)_{i1}$ and $(K_4)_{i1}$ are zero because of condition $\underline{R} \cdot \hat{n}' = 0$.) It is shown at the end of this section that the self-terms have a very simple form, i.e., $(K_1)_{ij} = c_o \Delta t$, $(K_3)_{ij} = c_i \Delta t$ independently of location and time. Notice that the two indices correspond to those in the left-hand sides of equations 20. Thus equations 21a can be solved to give

$$\psi_i^1 = \frac{s_i^1}{1 + c_o/c_i} = \frac{2(\psi^{inc})_i^1}{1 + c_o/c_i}$$

$$\phi_i^{1/2} = \frac{1}{c_i \Delta t}\, \psi_i^1.$$

At the next time step, i.e., $t = 2\tau$ equations 20 can be rewritten as

$$\psi_i^2 = s_i^2 - (K_1)_{i2}\, \phi_i^{3/2} - \sum_{k=1}^{N} \left[(K_1)_{k1}\, \phi_k^{1/2} + (K_2)_{k1}\, \dot{\psi}_k^{1/2} \right]$$

$$\psi_i^2 = (K_3)_{i2}\, \phi_i^{3/2} + \sum_{k=1}^{N} \left[(K_3)_{k1}\, \phi_k^{1/2} + (K_4)_{k1}\, \dot{\psi}_k^{1/2} \right]$$

where $(K_1)_{i2} = c_o \Delta t$, $(K_3)_{i2} = c_i \Delta t$. From $\dot{\psi}_k^{1/2} = (\psi_k^1 - \psi_k^0)/\Delta t$ all $\dot{\psi}_k^{1/2}$ are known since $\psi_k^0 = 0$ and ψ_k^1 are known from $t = \tau$. Also all $\phi_k^{1/2}$ are known from the $t = \tau$ step and the above system of equations can be solved for $\psi_i^2, \phi_i^{3/2}$. In general by marching on in time we can evaluate $\psi_i^j, \phi_i^{j-1/2}$ in terms of $s_i^j, \psi_k^\ell, \phi_k^{\ell-1/2}$ ($k = 1,2,\ldots,N$ and $\ell = 1,2,\ldots,j-1$) by inverting a 2 x 2 matrix.

The success of the above procedure depends among other factors on how well we can calculate the influence coefficients $\int_{All} K_p \, ds'dt'$ ($p = 1,2,3,4$). Fortunately, these integrals can be performed explicitly in terms of simple functions. From equations 19 we see that we have two types of integrals,

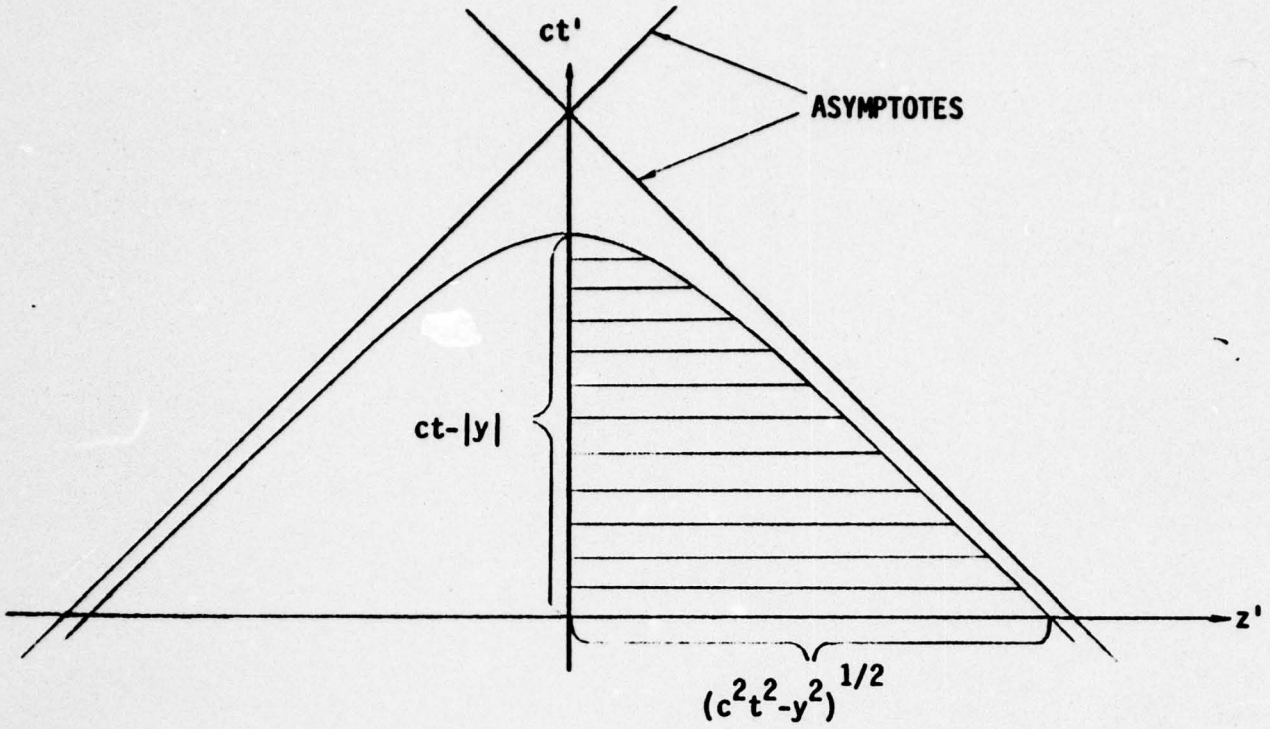

Figure 8. The Shaded Area Represents the Light "Cone" or Region of Influence for Points on the y=0 Side on Those on the z=0 Side of the Rectangular Cross Section (fig. 4)

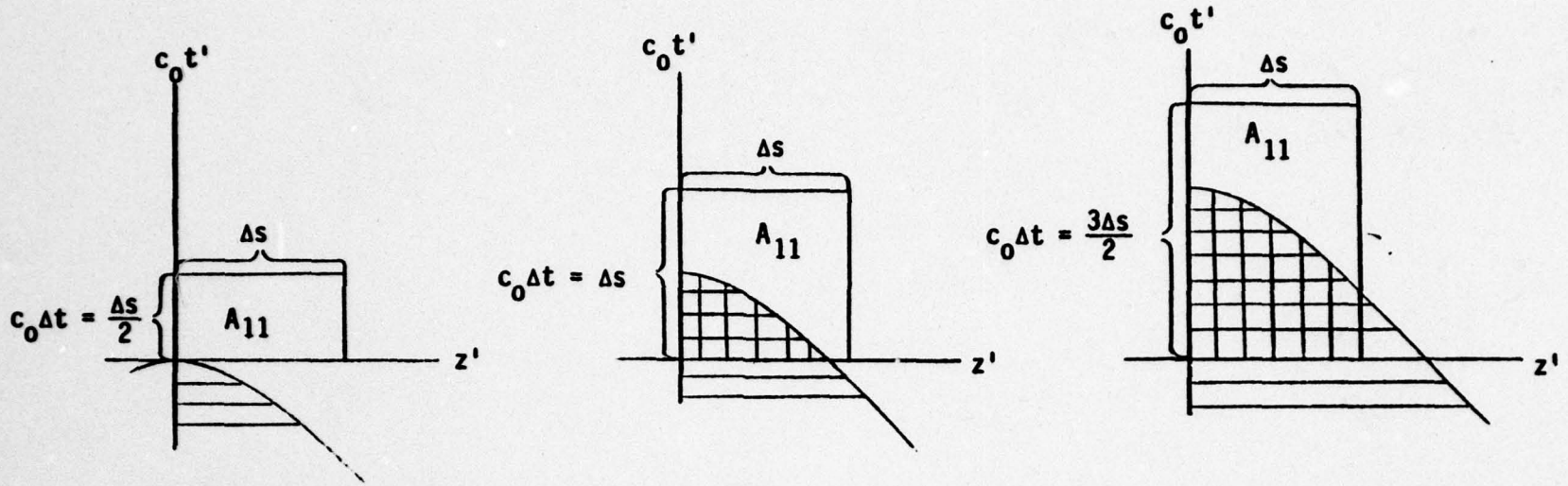

Figure 9. Diagrams Showing the Dependence of Influence Coefficients, for the Interaction of Line Segment 1 and the Midpoint of Line Segment N (fig. 5), on the Temporal Step Size Δt

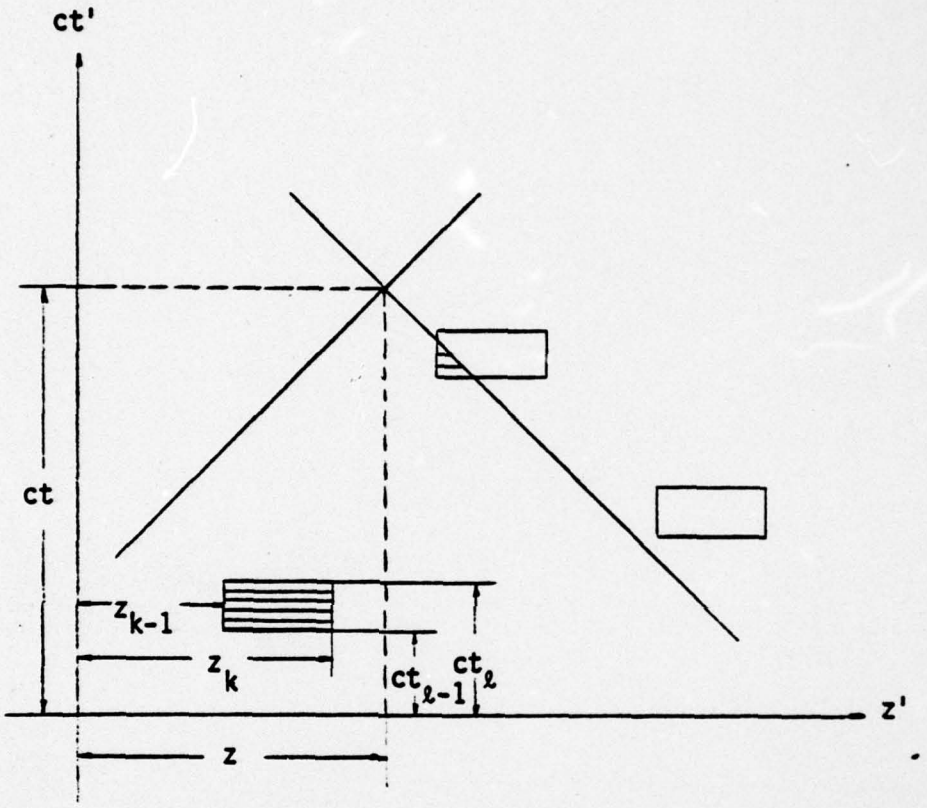

Figure 10. Geometry Illustrating the Influence of Line Segments of a Side (here the y=0 Side) on a Point on the Same Side. The Influence Coefficients are Zero if the Corresponding Zone Lies Entirely Outside the Light "Cone"

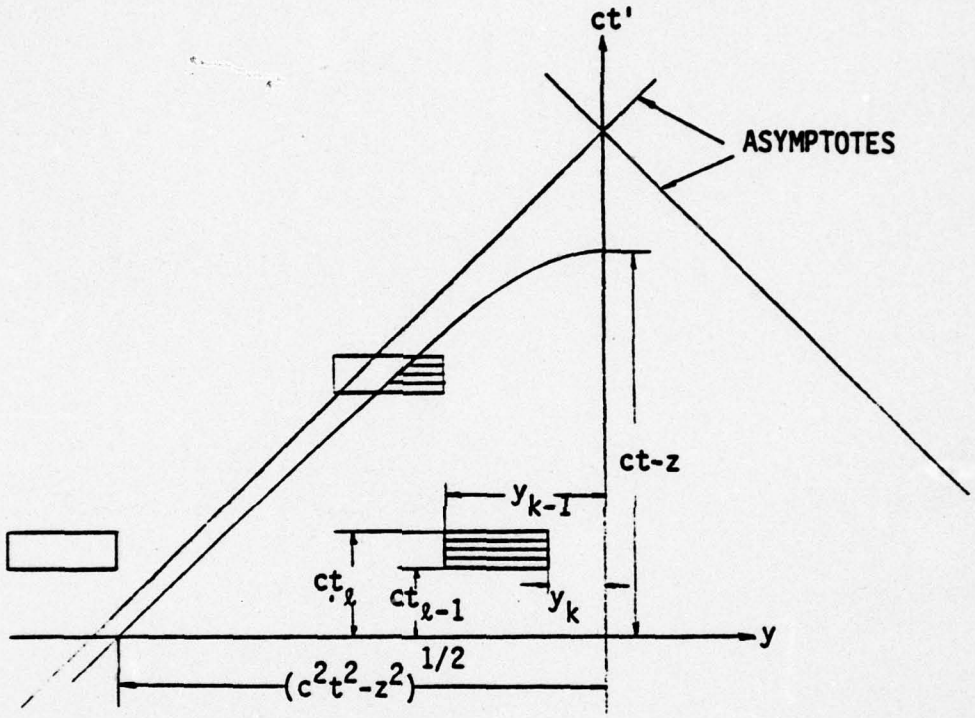

Figure 11. Geometry Illustrating the Influence of Line Segments of the z=0 Side on a Point on the y=0 Side. The Influence Coefficients are Zero if the Corresponding Zone Lies Entirely Outside the Light "Cone"

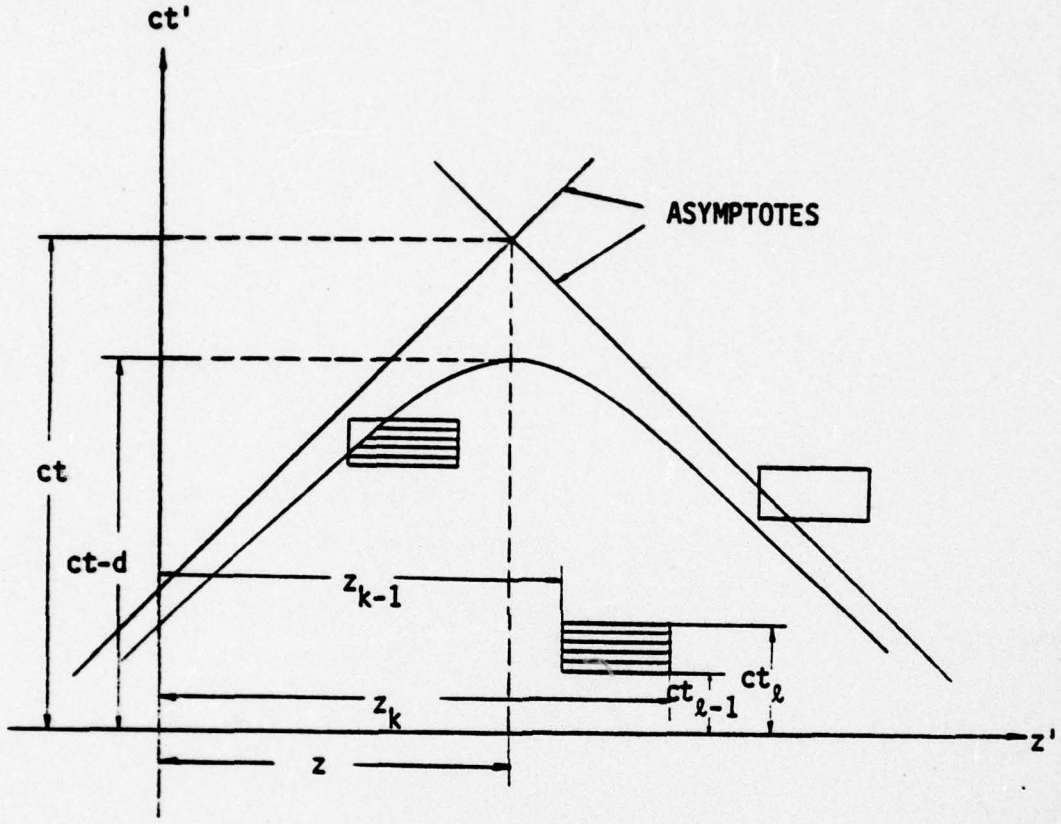

Figure 12. Geometry Illustrating the Influence of Line Segments of Side y=0 on a Point on Side y=-d. The Influence Coefficients are Zero if the Corresponding Zone Lies Entirely Outside the Light "Cone"

$$I_1 = \frac{c}{\pi} \int_A \frac{U[c(t - t') - R]}{\left[c^2(t - t')^2 - R^2\right]^{1/2}} \, ds'dt'$$

$$I_2 = \frac{c}{\pi} \int_A \frac{(\underline{R} \cdot \hat{n}')(t - t')}{R^2} \frac{U[c(t - t') - R]}{\left[c^2(t - t')^2 - R^2\right]^{1/2}} \, ds'dt' \qquad (23)$$

where c is c_o or c_i and A is a zone in the s,t space. As we mentioned ealrier, the presence of the step function U may alter the region of integration since U = 1 for $c(t - t') - R \geq 0$ and U = 0 for $c(t - t') - R < 0$. For example, on the same side of the rectangle, say y = 0 we have $R = |z - z'|$ and inequality $c(t - t') - |z - z'| \geq 0$ represents the light "cone" in the z',t' coordinate system (fig. 6). Thus if a zone intersects the light cone as shown in figure 10 the area over which integrations 22 are to be performed is the shaded part of A. As we indicated earlier, the light "cone" does not necessarily consist of straight lines. If, for example, the reference point lies on the y = 0 side and the integration points on the y = -d or z = 0 sides, then $R=[(z - z')^2 + d^2]^{1/2}$ or $R=[z'^2 + y^2]^{1/2}$ respectively and inequality $t - t' \geq R$ represents a region bounded by one branch of a hyperbola in the z',ct' or y',ct' coordinate systems respectively. These are the light "cones" for these cases. Again if the zone intersects the light "cone" (fig. 11, 12) only the shaded part of zone A will contribute to the integration. No matter what the relative position of the spatial reference and integration points is, inequality $c(t - t') \geq R$ represents a light "cone" or a region of influence and in the appropriate s',t' coordinate system there are, in our case, fifteen possible diagrams for the relative positions of the light

"cone" and a zone. In figure 13 only ten diagrams are presented since intersections of the light "cone" with zones occur symmetrically and only the right-hand off center ones are displayed. Also the light "cone" depicted can be hyperbolic or straight or both depending on the diagram. Notice that for each diagram the integration area is either a rectangle or a triangular region or a combination of the two. Thus we need only exhibit the results of integration for diagrams VII and XI (fig. 14). First we recall that when the reference and integration points lie on the same side of the rectangle the inner product $\underline{R} \cdot \hat{n}'$ is zero and I_1 defined in equation 22 is zero. Next, for convenience but without sacrificing generality we choose our integration points on the $y = 0$ side and the reference point on the $z = 0$ side, i.e., $\underline{R} = z' \hat{e}_z + y \hat{e}_y$, $R = (z'^2 + y^2)^{1/2}$. (If another combination is chosen, for example reference point on $z = b$ side, then $\underline{R} = (z' - b)\hat{e}_z + y \hat{e}_y$, $R = [(z' - b)^2 + y^2]^{1/2}$. A simple change of variables, $b = z' = z''$, can then reduce this case to the previous one by appropriately changing the limits of the z' integration. Similar agruments hold true for all other combinations.) Referring to figure 14 the following results can be obtained.

$$I_1(\text{VII}) = \frac{c}{\pi} \int_A \frac{U[c(t - t') - R]}{\left[c^2(t - t')^2 - R^2\right]^{1/2}} \, ds'dt'$$

$$= \frac{c}{\pi} \int_{t_{\ell-1}}^{t^*} \int_{z_{k-1}}^{z(t')} \frac{dz'dt'}{\left[c^2(t - t')^2 - z'^2 - y^2\right]^{1/2}}$$

where $z(t')$ is obtained by setting $c(t - t') - R = 0$, i.e., $z(t') = \left[c^2(t - t')^2 - y^2\right]^{1/2}$, $t^* = t - (1/c)(z_{k-1}^2 + y^2)^{1/2}$ and

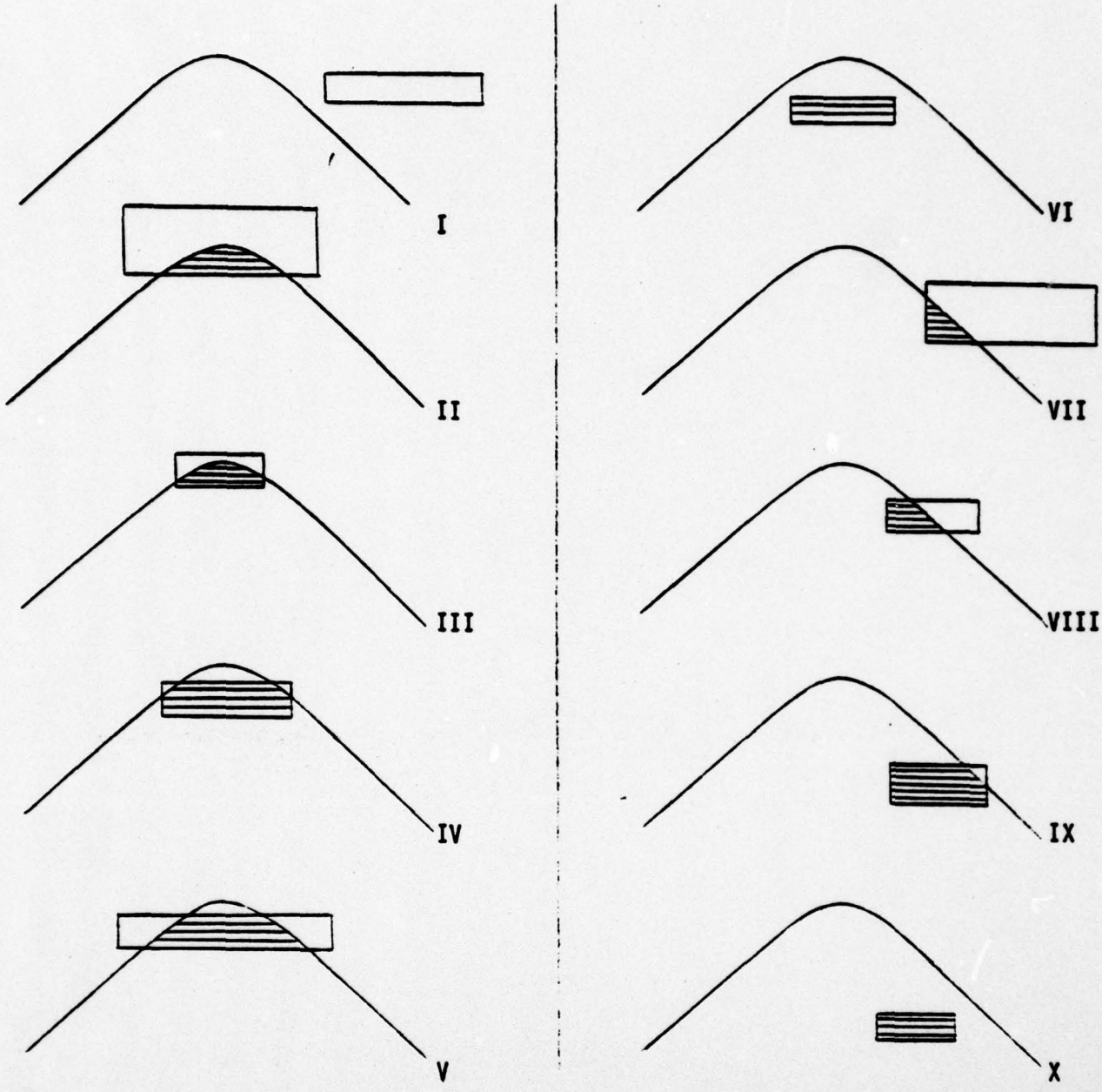

Figure 13. Diagrams Illustrating the Various Light "Cone"-Zone Intersections For Zones Off Center and Because of Symmetry Only the Right-Hand Intersections are Displayed

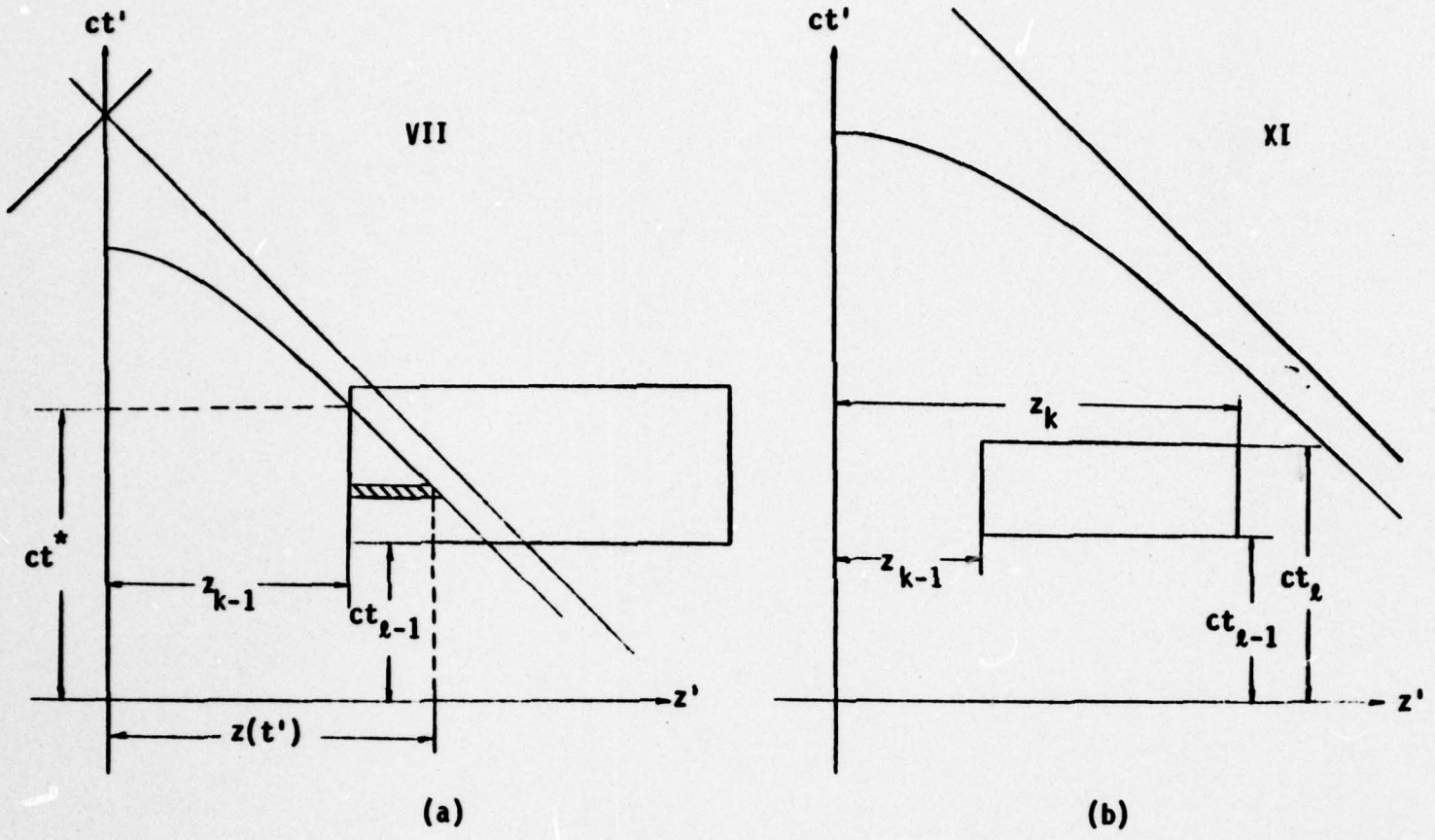

Figure 14. Geometry Relevant to the Calculation of Two Representative Influence Coefficients

$$I_1(\text{VII}) = \frac{1}{\pi}\left[c(t - t_{\ell-1})\tan^{-1}\frac{\sqrt{c^2(t - t_{\ell-1})^2 - z_{k-1}^2 - y^2}}{z_{k-1}}\right.$$

$$- z_{k-1}\log\left|\frac{\sqrt{z_{k-1}^2 + y^2}}{c(t - t_{\ell-1}) - \sqrt{c^2(t - t_{\ell-1})^2 - z_{k-1}^2 - y^2}}\right|$$

$$\left. - y\tan^{-1}\frac{y\sqrt{c^2(t - t_{\ell-1})^2 - z_{k-1}^2 - y^2}}{c(t - t_{\ell-1})\, z_{k-1}}\right] \qquad (24)$$

$$I_2(\text{VII}) = \frac{c}{\pi}\int_A \frac{\underline{R}\cdot\hat{n}(t - t')}{R^2}\,\frac{U[c(t - t') - R]}{[c^2(t - t')^2 - R^2]^{1/2}}\,ds'dt'$$

$$= \frac{c}{\pi}\int_{t_{\ell-1}}^{t^*}\int_{z_{k-1}}^{z(t')}\frac{y(t - t')\,dz'dt'}{(y^2 + z'^2)[c^2(t - t')^2 - z'^2 - y^2]^{1/2}}$$

where again $z(t') = [c^2(t - t')^2 - y^2]^{1/2}$, $t^* = t - (1/c)\cdot(z_{k-1}^2 + y^2)^{1/2}$ and

$$I_2(\text{VII}) = \frac{1}{\pi c}\left[c(t - t_{\ell-1})\tan^{-1}\frac{y\sqrt{c^2(t - t_{\ell-1})^2 - z_{k-1}^2 - y^2}}{c(t - t_{\ell-1})\, z_{k-1}}\right.$$

$$\left. - y\tan^{-1}\frac{\sqrt{c^2(t - t_{\ell-1})^2 - z_{k-1}^2 - y^2}}{z_{k-1}}\right] \qquad (25)$$

Similarly,

$$I_1(XI) = \frac{c}{\pi} \int_{t_{\ell-1}}^{t_\ell} \int_{z_{k-1}}^{z_k} \frac{dz'dt'}{[c^2(t-t')^2 - z'^2 - y^2]^{1/2}}$$

$$= \frac{1}{\pi} \left[-c(t-t') \tan^{-1} \frac{z'}{\sqrt{c^2(t-t')^2 - z'^2 - y^2}} \right.$$

$$+ z' \log \left| c(t-t') - \sqrt{c^2(t-t')^2 - z'^2 - y^2} \right|$$

$$\left. + y \tan^{-1} \frac{c(t-t')\, z'}{y\sqrt{c^2(t-t')^2 - z'^2 - y^2}} \right] \Bigg|_{z_{k-1}}^{z_k} \Bigg|_{t_\ell}^{t_{\ell+1}} \qquad (26)$$

where

$$f(z',t') \Big|_{z_{k-1}}^{z_k} \Big|_{t_{\ell-1}}^{t_\ell} = f(z_k,t_\ell) - f(z_{k-1},t_\ell)$$

$$- f(z_k,t_{\ell-1}) + f(z_{k-1},t_{\ell-1})$$

$$I_2(XI) = \frac{c}{\pi} \int_{t_{\ell-1}}^{t_\ell} \int_{z_{k-1}}^{z_k} \frac{y(t-t')\, dz'dt'}{(z'^2 + y^2)[c^2(t-t')^2 - z'^2 - y^2]^{1/2}}$$

$$= \frac{1}{\pi c} \left[c(t-t') \tan^{-1} \frac{c(t-t')\, z'}{y\sqrt{c^2(t-t')^2 - y^2 - z'^2}} \right.$$

$$\left. - y \tan^{-1} \frac{z'}{\sqrt{c^2(t-t')^2 - y^2 - z'^2}} \right] \Bigg|_{z_{k-1}}^{z_k} \Bigg|_{t_{\ell-1}}^{t_\ell} \qquad (27)$$

where again

$$f(z',t')\Big|_{z_{k-1}}^{z_k}\Big|_{t_{\ell-1}}^{t_\ell} = f(z_k,t_\ell) - f(z_{k-1},t_\ell)$$

$$- f(z_k,t_{\ell-1}) + f(z_{k-1},t_{\ell-1})$$

Finally we calculate, as promised, the <u>self-terms</u>

$$(K_p)_{ij} = \frac{c}{\pi}\int_A \frac{U[c(t-t') - R]}{[c^2(t-t')^2 - R^2]}\,ds'dt' \qquad (p=1,\ c=c_o;\ p=3,\ c=c_i)$$

where the reference point of zone A coincides with the apex of the light cone. The calculation of the self-terms does not depend on which side the line segment lies. Thus in figure 15 we have chosen side y = 0 and the above integral can be rewritten as

$$(K_p)_{ij} = \frac{2}{\pi}\int_0^{c\Delta t}\int_0^{v} \frac{dudv}{(v^2 - u^2)^{1/2}} = c\Delta t$$

where substitutions $c(t - t') = v$, $z' - z = u$ have been made.

In order to test the validity of the numerical solution obtained via the integral equation method, we calculated Ψ at the middle of the front side of the rectangular slab as a function of time and also Ψ on the top side of the slab as a function of z at a particular instant and compared them to solutions obtained with the finite difference method (FDM) which was being studied simultaneously. The agreement was

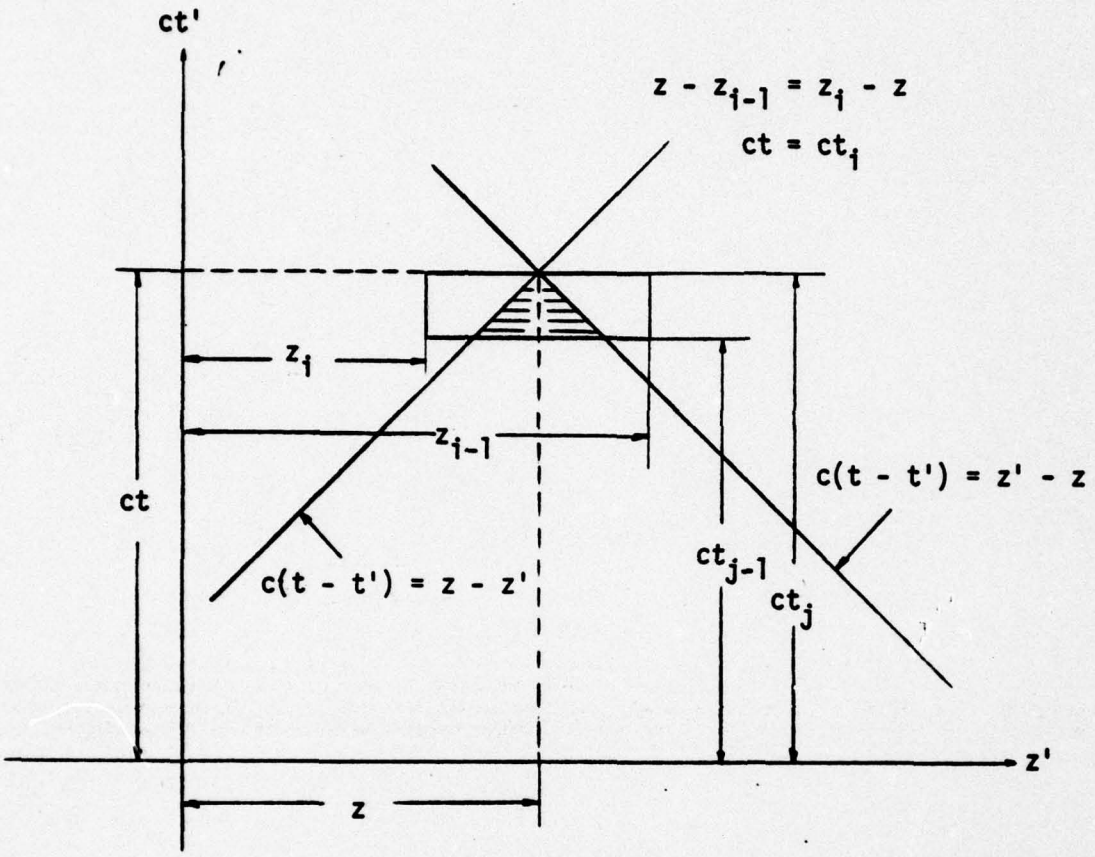

Figure 15. Geometry for the Calculation of Self-Terms in the Integral Equation Method

excellent and the relevant graphs (figs. 20 and 21) are presented in section V where the numerical results are discussed. At that time we had decided that the FDM was preferable for the calculations of interest (section VI offers a comparison of the two methods) and we proceeded to evaluate Ψ at points on the surface of the slab using the FDM. As additional debugging for the FDM we calculated Ψ for the problem of diffraction by a 90° perfectly conducting wedge and compared our results to the known exact solution. The agreement was again excellent and this spurred our curiosity to test the FDM for a wedge with a zero angle, i.e., a perfectly conducting half-plane. Once more the agreement was excellent and it suggested the very interesting possibility of tackling open surfaces with the FDM. In the next section we develop this method as applied to our two-dimensional scattering from a dielectric rectangular slab.

SECTION IV

FINITE DIFFERENCE METHOD

In order to apply a finite difference scheme to the solution of our scattering problem we can either employ equations 2 and 3 for E_x, H_y, H_z (option 1) or <u>one</u> equation for $E_x \equiv \Psi$ (option 2), namely equation 5. Option 1 allows us to solve for all field components simultaneously whereas option 2 only produces E_x and H_y, H_z must be obtained with the aid of equations 2. However, there is a clear advantage of option 2 that prompted us to choose it: We know that for a perfectly conducting wedge (P.C.W.) H_y and H_z diverge at the edge whereas E_x is zero. We want to use the P.C.W. for debugging and consequently we should use E_x alone which for our problem is also finite at the edge. H_y and H_z may or may not diverge for a dielectric body but in any case debugging with the aid of the P.C.W. might not be reliable since the divergence of H_y, H_z could introduce significant errors. We could try to provide special treatment near the edges but option 2 makes this unnecessary. In connection with the edge behavior one may wonder whether $\nabla^2_{yz}E_x$ in equation 5 diverges. To answer this we observe that this quantity is equal to $(1/c^2)(\partial^2 E_x/\partial t^2)$. E_x is finite for all times and therefore so is $\partial^2 E_x/\partial t^2$--if pathological functions are excluded. Thus $\nabla^2_{yz}E_x$ is indeed finite. Notice that as we cross the boundary, whether on the sides or at the corners, $\nabla^2_{yz}E_x$ suffers a discontinuity since c is discontinuous and $\partial^2 E_x/\partial t^2$ is continuous (due to the continuity of E_x for all times). The continuity of $c^2\nabla^2_{yz}E_x$ will allow us, later on in this section, to determine the proper finite difference scheme for this quantity as we cross the boundary.

Next we proceed to apply the finite difference method to equation 5 in a source-free region,

$$c^2 \nabla^2_{yz} \Psi(\underline{\rho},t) = \frac{\partial^2}{\partial t^2} \Psi(\underline{\rho},t), \qquad \underline{\rho} \in V \tag{5}$$

with appropriate boundary and initial conditions. V stands for the two-dimensional region bounded by a contour C_b (fig. 16) and it is divided by the contour C into an exterior region V_o and an interior region V_i. If V were a homogeneous region then the solution of equation 5 could be uniquely determined at a given time t and position $\underline{\rho}$ if the initial values of Ψ and $\dot{\Psi}$ were known everywhere within V and Ψ on C_b was known for all times up to t. To ensure uniqueness of $\Psi(\underline{\rho},t)$ in our case, the continuity of Ψ and $\partial\Psi/\partial n$ across the boundary C must be added to the boundary and initial conditions above. One may wonder, however, what this condition means when $\partial\Psi/\partial n$ is evaluated at an edge where it may diverge. To answer this we recall the system of integral equation 11 and observe that because the singularity of $\partial\Psi/\partial n$ is integrable we can remove the requirement of continuity of $\partial\Psi/\partial n$ at the four corners (i.e., four isolated points). We still obtain a unique solution for $\Psi(\underline{\rho},t)$.

Equation 5 is a hyperbolic equation and its solution via the method of finite differences has been extensively studied when V is homogeneous (see for example references 2 and 3). The method is stable and converges to the exact solution

---

2. Forsythe, G. E. and W. R. Wasow, Finite-Difference Methods for Partial Differential Equations, New York, John Wiley, 1960.

3. Fox, P., "The Solution of Hyperbolic Partial Differential Equations by Difference Methods," Mathematical Methods for Digital Computers, Edited by A. Ralston and H. S. Wilf, New York, John Wiley, 1964.

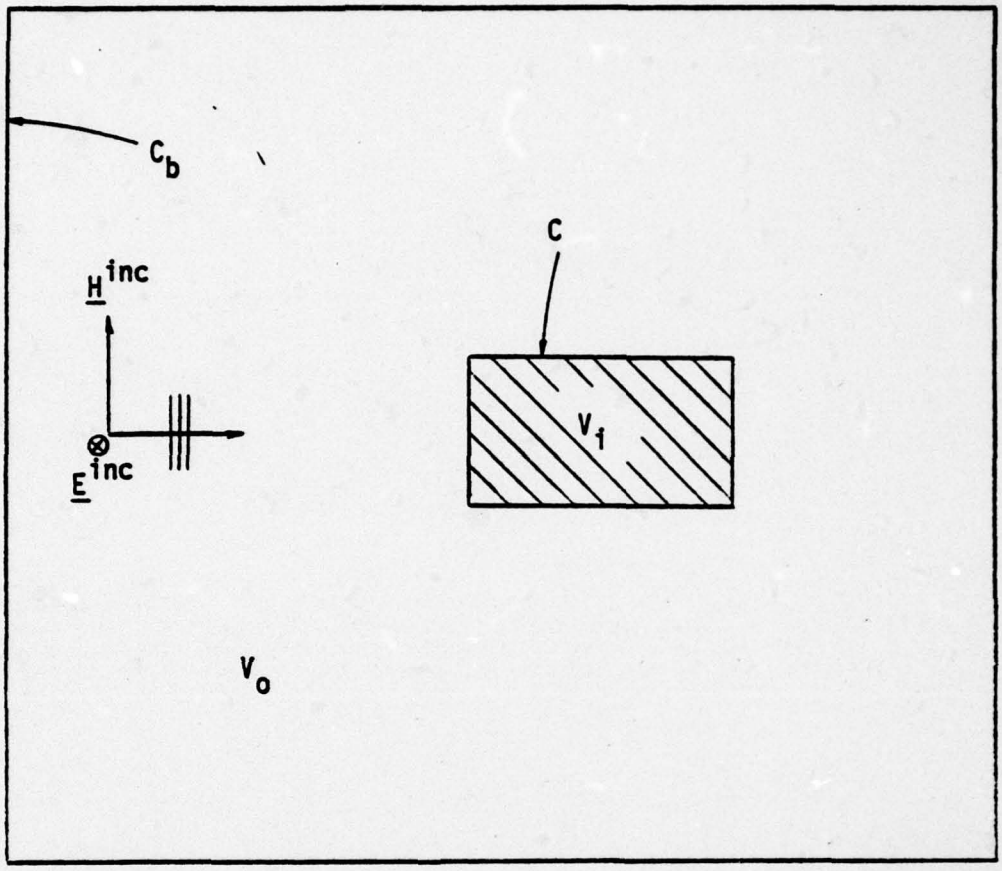

Figure 16. Geometry Depicting Boundaries C_b, C and Regions V_o, V_i

when $(c\tau/h_y)^2 + (c\tau/h_z)^2 < 1$, where τ is the temporal step size and h_y, h_z are the grid step sizes in the y and z directions respectively. For our scattering problem the finite difference method is still applicable provided the appropriate stability and convergence criteria and boundary and initial conditions are satisfied. In each region the stability and convergence criteria are: $(c_o\tau_o/h_{oy})^2 + (c_o\tau_o/h_{oz})^2 < 1$ and $(c_i\tau_i/h_{iy})^2 + (c_i\tau_i/h_{iz})^2 < 1$ outside and inside the rectangle respectively. It is desirable to choose $\tau_i = \tau_o$ and $h_{iy} = h_{oy}$, $h_{iz} = h_{oz}$ in which case both criteria are satisfied if $(c_o\tau_o/h_{oy})^2 + (c_o\tau_o/h_{oz})^2 < 1$ since $c_i < c_o$. The boundary and initial conditions are those we mentioned earlier in connection with the uniqueness of the solution of equation 5. (To verify the accuracy of the values at the interface C we compared the fields calculated via the finite difference approach and the integral equation method and the excellent agreement we obtained strongly indicated that the values were indeed accurate.) In the present case the incident plane wave pulse has a smooth wavefront and is assumed to hit the front side of the rectangle at t = 0. Thus Ψ and $\dot{\Psi}$ at t = 0 are known everywhere within V. Since derivatives are replaced by finite differences we write $\dot{\Psi}(\underline{\rho},o) = [\Psi(\underline{\rho},o) - \Psi(\underline{\rho},-\tau)]/\tau$ and the initial conditions are then translated into the statement "Ψ at $t = 0,-\tau$ is known everywhere within V." As we shall see later the finite difference method makes explicit use of this statement. The importance of the boundary condition will become evident as we transform equation 5 into a system of difference equations. In order to accomplish this we first replace region V by an orthogonal grid with grid sizes h_y and h_z as shown in figure 17. Notice that both C_b and C coincide with grid bars and the points at which Ψ will be evaluated coincide with the intersections of the grid bars. Next we introduce a temporal step size equal to τ and replace $\nabla^2_{yz}\Psi = (\partial^2\Psi/\partial y^2) + (\partial^2\Psi/\partial z^2)$ and

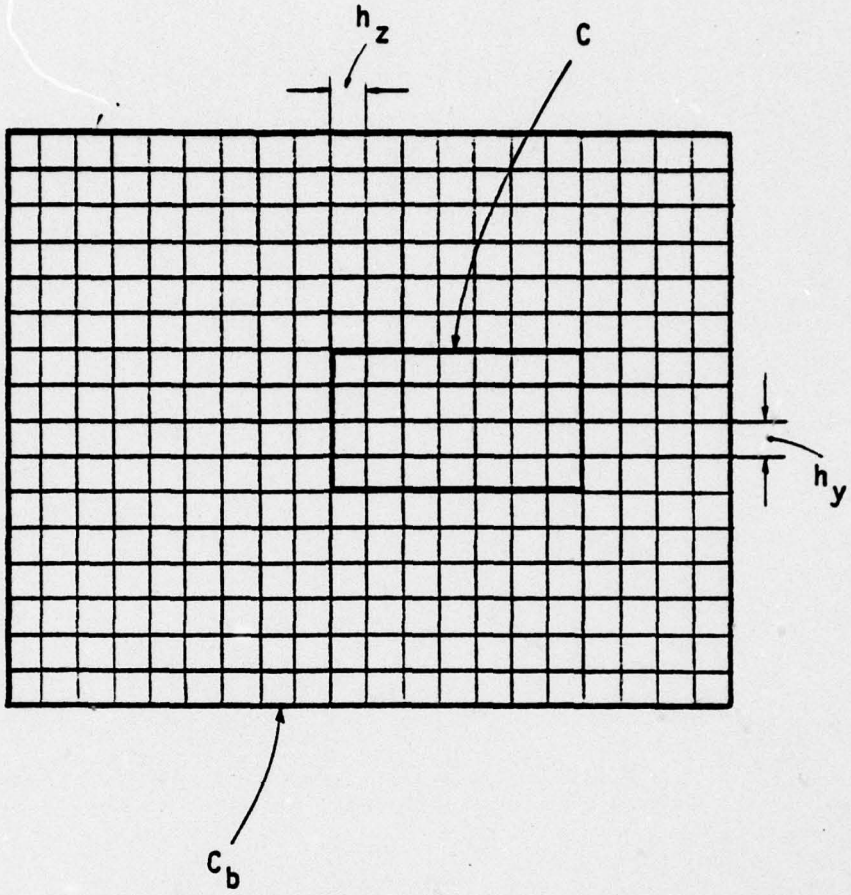

Figure 17. The Grid Used in the Finite Difference Method. The Boundaries Coincide with Grid Bars and the Observation Points with the Intersections of the Grid Bars

$\partial^2\Psi/\partial t^2$ by their appropriate differences in a region of homogeneity,

$$\frac{\partial^2}{\partial y^2}\Psi(\underline{\rho},t) = [\Psi(y + h_y,z,t) + \Psi(y - h_y,z,t) - 2\Psi(y,z,t)]/h_y^2 + O(h_y)$$

$$\frac{\partial^2}{\partial z^2}\Psi(\underline{\rho},t) = [\Psi(y,z + h_z,t) + \Psi(y,z - h_z,t) - 2\Psi(y,z,t)]/h_z^2 + O(h_z)$$

$$\frac{\partial^2}{\partial t^2}\Psi(\underline{\rho},t) = [\Psi(y,z,t + \tau) + \Psi(y,z,t - \tau) - 2\Psi(y,z,t)]/\tau^2 + O(\tau). \qquad (28)$$

Equations 28 would be exact if $\Psi(\underline{\rho},t)$ were a quadratic function of y, z, and t. In our subsequent calculations we set $h_y = h_z = h$ because the back side of the rectangle (z = -b) will be taken sufficiently far from the front side (z = 0) so it will have no effect on our field calculations for the time periods of interest. (Thus we define h by dividing the front side into equal-sized segments and the top side is set equal to an integer multiple of h.) The next two steps involve the boundary conditions across C and specifying Ψ on C_b. The boundary conditions across C require continuity of Ψ and $\partial\Psi/\partial n$. As we observed earlier in this section $c^2\nabla_{yz}^2\Psi$ is also continuous. These three conditions will alow us to replace $c^2\nabla_{yz}^2\Psi$ by a difference scheme for points on the sides of the rectangle. We begin with point $\underline{\rho}$ on side y = 0 and for convenience we choose a coordinate system yz with origin at $\underline{\rho}$ and set t = 0. (This choice for t has nothing to do with previous considerations and it is only a matter of convenience. Our results will be valid for any t.) We will assume as we did

for the derivation of equations 28 that Ψ can be expanded in a Maclaurin series about $z = 0$, $y = 0$.

$$\Psi_o = a + by + cz + dy^2 + ez^2 + fyz + O(h^3) \qquad y > 0$$

$$\Psi_i = a' + b'y + c'z + d'y^2 + e'z^2 + f'yz + O(h^3) \qquad y < 0 \tag{29}$$

Ψ and $\partial\Psi/\partial n = \partial\Psi/\partial y$ are continuous as we cross $y = 0$, i.e., $a = a'$, $b = b'$, $e = e'$, $c = c'$, $f = f'$. To determine the relationship between d and d' we recall that $c^2\nabla^2_{yz}\Psi$ is also continuous as we cross $y = 0$, i.e.,

$$c_o^2\nabla^2_{yz}\Psi_o = (2d + 2e)c_o^2 = c_i^2\nabla^2_{yz}\Psi_i = c_i^2(2d' + 2e')$$

and

$$d' = (d + e)\,\frac{c_o^2}{c_i^2} - e. \tag{30}$$

In order to determine the difference expression for $c^2\nabla_{yz}\Psi$ at $y = z = ct = 0$ we set

$$c^2\nabla_{yz}\Psi = \frac{1}{h^2}\,[A\Psi(h,0,0) + B\Psi(-h,0,0) + C\Psi(0,0,0)]$$

$$+ \frac{1}{h^2}\,[D\Psi(0,h,0) + E\Psi(0,-h,0) + F\Psi(0,0,0)]$$

$$= 2(d + e)\,c_o^2. \tag{31}$$

Using equations 29, equation 31 gives

$$A(a + bh + dh^2) + B\left[a - bh + \left[(d + e)\frac{c_o^2}{c_i^2} - e\right]h^2\right] + Ca$$

$$+ D(a + ch + eh^2) + E(a - ch + eh^2)$$

$$+ Fa = 2(d + e)\, c_o^2 h^2. \qquad (32)$$

Setting the coefficients of a, b, c, d and e in equations 32 equal to zero we obtain

$$A + B + C + D + E + F = 0$$

$$(A - B)h = 0$$

$$(D - E)h = 0$$

$$\left(A + B\frac{c_o^2}{c_i^2} - 2c_o^2\right)h^2 = 0$$

$$\left[D + E + B\left(\frac{c_o^2}{c_i^2} - 1\right) - 2c_o^2\right]h^2 = 0$$

i.e.,

$$A = B = E = D = \frac{2c_o^2}{1 + \frac{c_o^2}{c_i^2}}$$

$$C + F = -\frac{8c_o^2}{1 + \frac{c_o^2}{c_i^2}}. \qquad (33)$$

Thus the difference formula for $c_o^2\nabla_{yz}^2\Psi_o = c_i^2\nabla_{yz}^2\Psi_i$ on the boundaries of the rectangle is

$$c_o^2\nabla_{yz}^2\Psi_o = c_i^2\nabla_{yz}\Psi_i = \frac{2c_o^2}{1 + \frac{c_o^2}{c_i^2}}\Big[\Psi(y + h,z,t) + \Psi(y - h,z,t)$$

$$+ \Psi(y,z + h,t) + \Psi(y,z - h,t) - 4\Psi(y,z,t)\Big]/h^2 \qquad (34)$$

where y,z is some point on the boundary C. Notice that our boundary includes the four corners and the question arises as to what the difference formula for $c^2\nabla_{yz}^2\Psi$ is at a corner. The answer is that since $c^2\nabla_{yz}^2\Psi$ is continuous we can choose an exterior point that is arbitrarily close to the corner and use the first two of equations 28 with $c = c_o$.

We are now in a position to replace equation 5 by a system of difference equations and examine the boundary conditions for Ψ on the outer boundary C_b. For a point away from the boundaries equation 5 assumes the form

$$\left(c^2(y,z)\tau^2/h^2\right)[\Psi(y + h,z,t) + \Psi(y - h,z,t) + \Psi(y,z + h,t)$$

$$+ \Psi(y,z - h,t) - 4\Psi(y,z,t)] = \Psi(y,z,t + \tau)$$

$$+ \Psi(y,z,t - \tau) - 2\Psi(y,z,t) \qquad (35)$$

where points $(y \pm h,z)$, $(y,z \pm h)$ lie in the same medium as y,z. Notice that equation 35 allows the determination of Ψ at $\underline{\rho},t + \tau$ in terms of the value of Ψ at $\underline{\rho}$ and neighboring points at earlier times. For a point on the boundary C equation 34 combined with the third of equation 28 replaces equation 5. Let us see how we can evaluate Ψ at a given

point and time. For simplicity let us assume that the front side of the rectangle extends to infinity, i.e., coincides with the z = 0 plane. This makes Ψ independent of y and the problem becomes one-dimensional ($\partial/\partial y = 0$). We define our region of interest by drawing two boundary walls $z = z_1 > 0$, $z = z_2 < 0$ and specifying Ψ on them. Thus we set $\Psi(z_1,t_o) = 0$ and $\Psi(z_2,t_o) = \Psi^{inc}(z_2,t_o)$. Obviously these conditions cannot be valid for any t_o since the reflected and transmitted waves will eventually reach the walls $z = z_2$ and $z = z_1$ respectively. Let us now select a point $z < 0$ and employ equation 35

$$(c_o^2\tau^2/h^2)[\Psi(z + h,t - \tau) + \Psi(z - h,t - \tau) - 2\Psi(z,t - \tau)]$$

$$= \Psi(z,t) + \Psi(z,t - 2\tau) - 2\Psi(z,t - \tau) \qquad (36)$$

We observe that $\Psi(z,t)$ depends on the value of Ψ at neighboring points at times less then t. Ψ at a neighboring point at $t - \tau$ can be similarly evaluated by writing equations analogous to 36 and it too depends on the values of Ψ at neighboring points at earlier times. This procedure shows that $\Psi(z,t)$ depends on $\Psi(z_2,t - n_2\tau)$ and $\Psi(z_1,t - n_1\tau)$ where $|z_2 - z| = n_2h$ and $z_1 - z = n_1h$. Thus if the walls have not been reached by the scattered waves at $\underline{t - n_2\tau}$ (for $z = z_2$) and $\underline{t - n_1\tau}$ (for $z = z_1$), the boundary conditions are valid and so is the calculation of Ψ at z and $\underline{t}$. Equation 36 shows that $\Psi(z,t)$ not only depends on the value of Ψ at neighboring points at $t - \tau$ but also on the value at Ψ at z at $t - \tau$ and $t - 2\tau$, i.e., a knowledge of these values is required which in turn depend on the value of Ψ at earlier times. This continues until we reach the initial conditions. Thus the difference scheme works as follows. First we write equations 36 and 34 at $t = \tau$

$$(c_i^2\tau^2/h^2)[\Psi(z_1,0) + \Psi(z_1 - 2h,0) - 2\Psi(z_1 - h,0)] = \Psi(z_1 - h,\tau)$$

$$+ \Psi(z_1 - h,-\tau) - 2\Psi(z_1 - h,0) \qquad z = z_1 - h$$

$$(c_i^2\tau^2/h^2)[\Psi(z + h,0) + \Psi(z - h,0) - 2\Psi(z,0)] = \Psi(z,\tau)$$

$$+ \Psi(z,-\tau) - 2\Psi(z,0) \qquad z > 0$$

$$\frac{2c_o^2\tau^2}{h^2(1 + c_o^2/c_i^2)}[\Psi(h,0) + \Psi(-h,0) - 2\Psi(0,0)] = \Psi(0,\tau)$$

$$+ \Psi(0,-\tau) - 2\Psi(0,0) \qquad z = 0$$

$$(c_o^2\tau^2/h^2)[\Psi(z + h,0) + \Psi(z - h,0) - 2\Psi(z,0)] = \Psi(z,\tau)$$

$$+ \Psi(z,-\tau) - 2\Psi(z,0) \qquad z < 0$$

$$(c_o^2\tau^2/h^2)[\Psi(z_2 + 2h,0) + \Psi(z_2,0) - 2\Psi(z_2 + h,0)] = \Psi(z_2 + h,\tau)$$

$$+ \Psi(z_2 + h,-\tau) - 2\Psi(z_2 + h,0) \qquad z = z_2 + h \quad (37)$$

where $z = z_1 > 0$ and $z = z_2 < 0$ are the two boundary walls such that $\Psi(z_1,t) = 0$, $\Psi(z_2,t) = \Psi^{inc}(z_2 t)$. Notice that equations 37 show that $\Psi(z,\tau)$, for any z (except at the boundaries), depends on $\Psi(z \pm h,0)$, $\Psi(z,0)$ and $\Psi(z,-\tau)$, i.e., on the initial values ($t = 0,-\tau$) of Ψ everywhere within V. These values are known as we explained earlier, i.e., equations 37 allow the calculation of $\Psi(z,\tau)$ everywhere. At this point the boundary conditions are superseded by the initial conditions but they will manifest themselves in the next step which involves a set of equations similar to equations 37 written at $t = 2\tau$ rather than $t = \tau$. This

new set allows the calculation of $\Psi(z,2\tau)$ in terms of $\Psi(z \pm h,\tau)$, $\Psi(z,\tau)$ that were calculated in the first step and $\Psi(z,0)$ that is known through the initial condition. Notice that the first and last of equations 37 written at $t = 2\tau$ involve $\Psi(z_1,\tau)$ and $\Psi(z_2,\tau)$ respectively, i.e., the values of Ψ at the boundaries. These values were not calculated in the first step; they have to be specified. It is clear now that we can march on in time in steps of τ and calculate $\Psi(\pm mh,n\tau)$ for any m and n provided the boundary conditions are not violated.

The simple one-dimensional scattering problem above, well illustrates the mechanics of the difference equation method. Our two-dimensional scattering problem can be solved similarly subject to appropriate initial and boundary conditions. The initial conditions still require knowledge of $\Psi(y,z,0)$ and $\Psi(y,z,-\tau)$ everywhere and the boundary conditions now involve four walls instead of two, i.e., $y = y_1,y_2$ in addition to $z = z_1,z_2$. The boundary conditions at $z = z_1,z_2$ are still $\Psi(z_1,t) = 0$ and $\Psi(z_2,t) = \Psi^{inc}(z_1,t)$. In the y direction the symmetry about the $y = y_m < 0$ plane, where y_m is the y coordinate of the middle of the front side, allowed us to impose the condition $\Psi(y_m - h,z,t) = \Psi(y_m + h,z,t)$, where $y = y_m - h$ is the boundary wall, and it works as follows. The difference equation at y_m,z,t is

$$\gamma[\Psi(y_m + h,z,t - \tau) + \Psi(y_m - h,z,t - \tau) - 2\Psi(y_m,z,t - \tau)]$$

$$= \Psi(y_m,z,t) + \Psi(y_m,z,t - 2\tau) - 2\Psi(y_m,z,t - \tau)$$

where γ depends on z. Because of the boundary condition $\Psi(y_m + h,z,t - \tau) = \Psi(y_m - h,z,t - \tau)$, $\Psi(y_m,z,t)$ can be calculated in terms of the value of Ψ evaluated at earlier times. For example, $\Psi(y_m,z,2\tau)$ is calculated in terms of $\Psi(y_m,z,\tau)$ and $\Psi(y_m + h,z,\tau)$ which were evaluated in the

first ($t = \tau$) step and $\Psi(y_m,z,0)$ which is known through the initial condition. Notice that the above boundary condition is true for all times in contradistinction to the boundary conditions at $z = z_1,z_2$. Finally, the second boundary condition in the y direction is imposed by assuming that $\Psi(y_p + h,z,t) = \Psi(y_p - h,z,t)$ where $y = y_p + h$ is the second boundary wall in the y direction and y_p (as well as z_1 and z_2) depends on the period of time over which we wish to know Ψ. This condition means that our scattering configuration is periodic in the y direction which of course is not true. It is just a convenient condition and it will be violated when the scattered wave reaches the wall. Again the calculation of Ψ at y,z,t will depend on the value of Ψ at the boundary at $t - nh$ where $y_p - y = (n - 1)h$. The violation of conditions $\Psi(y,z_2,t) = \Psi^{inc}(y,z_2,t)$ and $\Psi(y_p + h,z,t) = \Psi(y_p - h,z,t)$ will not be readily noticed because the scattered field has a smooth wavefront that builds up slowly and at the time of the violation the incident field may have a high value. However, the violation of condition $\Psi(y,z_1,t) = 0$ corresponding to a perfectly conducting wall at $z = z_1$ will be quickly felt in its vicinity. We can easily keep track of these violations in the computer printout and discard erroneous results.

As we explained at the end of section III we debugged the finite difference method by (a) testing surface field calculations, for scattering by a dielectric rectangular slab, obtained via this method against analogous calculations obtained via the integral equation method and (b) by comparing field calculations off the surface of a 90° perfectly conducting wedge and a perfectly conducting half-plane, both illuminated by a plane electromagnetic pulse, with the known exact solutions. In all instances the agreement was excellent. The relevant graphs are given in the next section where all the numerical results are presented.

Finally, we mention that the boundary condition given by equation 34 was not critical in applying the finite difference scheme to our problem. That is, by shifting the grid a little so that a grid bar was just in front of the interface and by applying the difference scheme given by equation 28 we obtained results of comparable accuracy to those obtained with the application of boundary condition 34. The only difference was that the interface could not be located to within a grid step size but this uncertainty can be reduced by making the step size smaller.

SECTION V

NUMERICAL RESULTS

In this section we present our numerical results in the form of graphs for field calculations on and off the surface of a rectangular dielectric slab illuminated by plane wave electromagnetic pulses with smooth wavefronts (fig. 4). We also present graphs, used for debugging, that show the excellent agreement between calculations obtained via the finite difference method and exact solutions for diffraction by 0° and 90° perfectly conducting wedges. Finally, we determine the time interval over which our slab results are applicable to the ATLAS I trestle platform problem.

In order to apply the finite difference method to diffraction by a perfectly conducting wedge we employed the scheme developed in the previous section and set $c_i = 0$, i.e., $\varepsilon_i/\varepsilon_o = \infty$. This is tantamount to setting $\Psi = 0$ for all times on the surface of the wedge. In order to test our numerical results we employed the known exact solutions for illumination by a plane wave step pulse and appropriately convolved these solutions with an incident pulse of our choice, i.e.,

$$E^{inc} = \Psi^{inc} = \frac{1600}{\beta^4} (c_o t)^2 (c_o t - \beta)^2 \, U(c_o t) \, U(\beta - c_o t). \tag{38}$$

This pulse starts at $t = 0$ and terminates at $t = \beta/c_o$ with a maximum of 100 (arbitrary units) at $t = \beta/2c_o$. It has a smooth wavefront with $\partial\Psi^{inc}/\partial t = 0$ at $t = 0$. A plot of the incident pulse is given in figure 19 with $\beta = 2.2$ (arbitrary units). Figures 18 and 19 exhibit the excellent agreement between the numerical results and the exact solutions. The spatial and temporal step sizes we used were $h = 0.05$, $c_o\tau = 0.025$, both in the same arbitrary units as β. Notice that

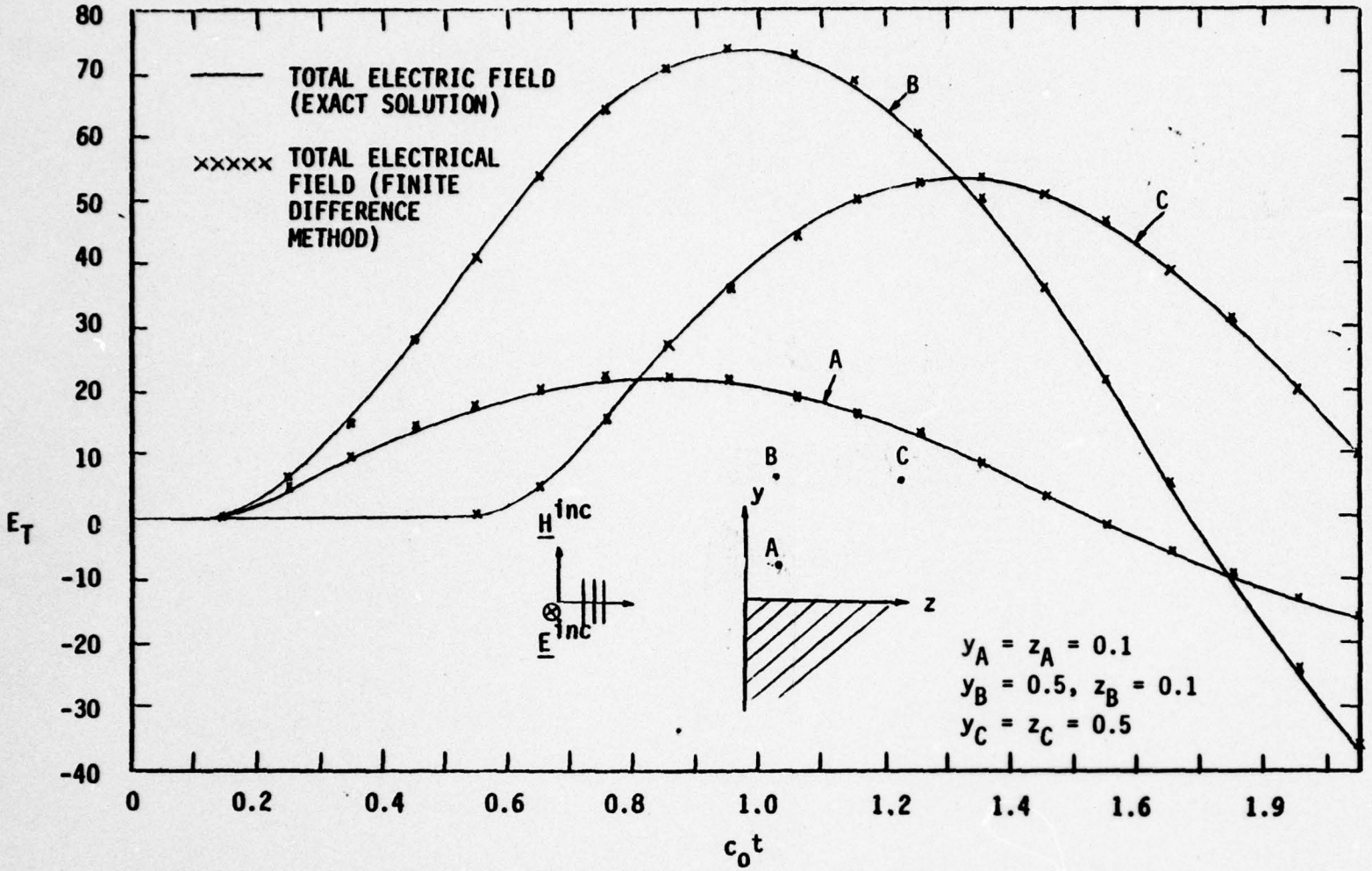

Figure 18. Comparison of Finite Difference Method Solution to Exact Solution for Diffraction by a 90° Perfectly Conducting Wedge. Units for Field Strength and $c_o t$ are Arbitrary. The Incident Field is Depicted in Figure 17

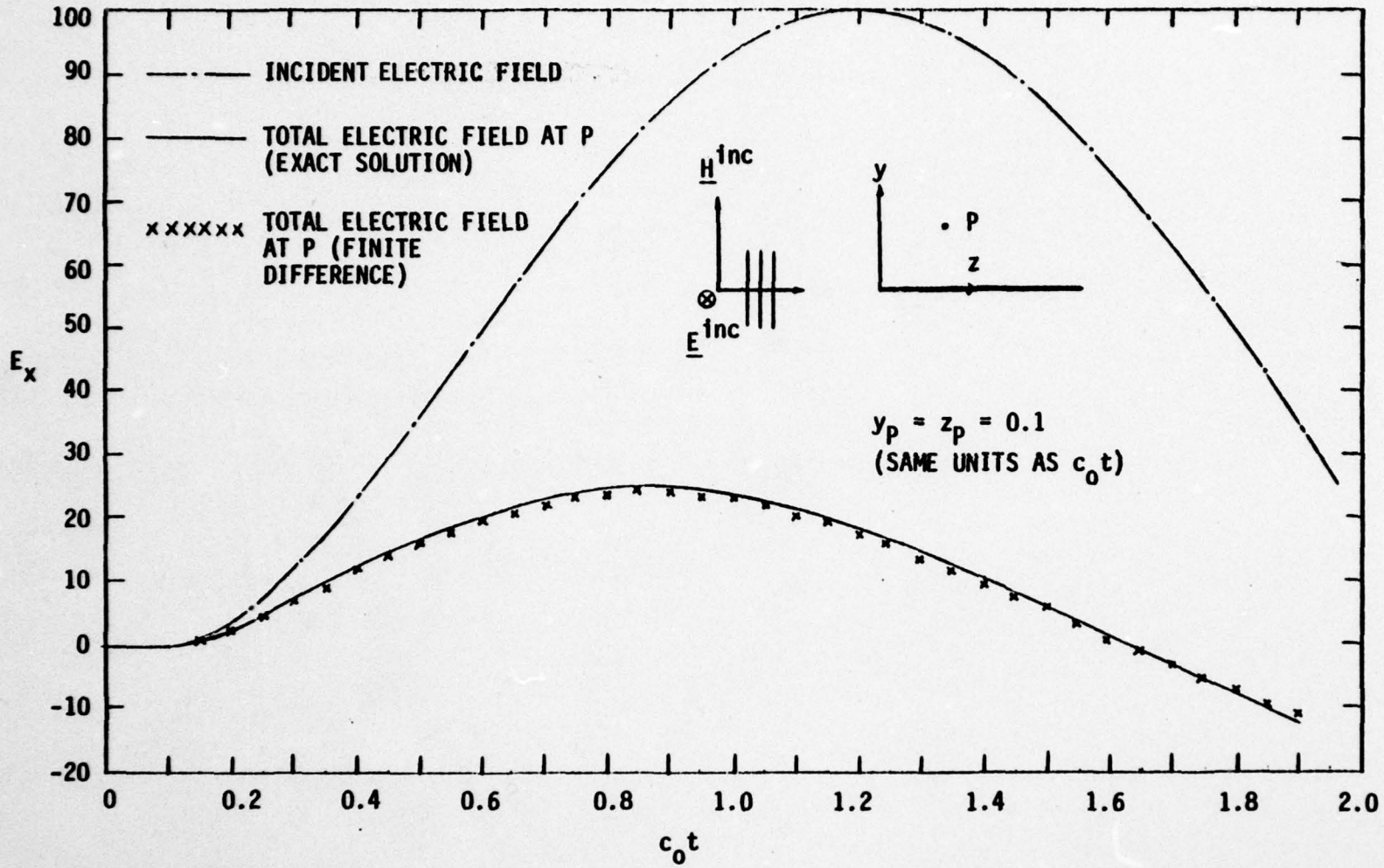

Figure 19. Comparison of Finite Difference Method Solution to Exact Solution for Scattering from a Perfectly Conducting Half-Plane. Units for Field Strength and $c_0 t$ are Arbitrary

the observation point (0.1,0.1) is only two spatial step sizes (in both the y and z directions) away from the edge but the agreement is still excellent.

The next two graphs present a comparison between the integral equation method and the finite difference method. In figure 20 we plotted the total electric field at the middle of the front side of the slab versus $c_o t/d$ where d is the thickness of the slab. The incident field is still given by equation 38 with $\beta = 2d$ and the slab has a dielectric constant $\varepsilon_i/\varepsilon_o = 4$, i.e., $c_i = c_o/2$. For the integral equation method we chose $\Delta s = d/8$ and $c_o \Delta t = h/2$ and for the finite difference method we chose $h = d/21$ and $c_o \tau = h/2$. We wanted to make the finite difference method as accurate as possible in order to compare it to the integral equation method and this is why we chose a finer spatial division for the former than the latter method. Figure 21 shows a comparison between the two methods for the total field evaluated on the top side ($y = 0$) of the slab versus z/d at an instant such that the incident wavefront has just arrived at $z = 4d$. The incident field is also plotted and occupies a length of two slab thicknesses since $\beta = 2d$. (For this case we chose $h = 2c_o \tau = d/21$ and $\Delta s = 2c_o \Delta t = d/6$.) The agreement between the integral equation method and the finite difference scheme is excellent and this served as debugging for both approaches.

The subsequent graphs present field calculations via the finite difference method at points off the surface of the slab. It was determined that for these calculations the finite difference method was superior to the integral equation method because of a lesser use of computational resources (see section VI). The incident field was chosen as a fast rising and slowly decaying pulse in order to emulate the electromagnetic pulse arising from an exoatmospheric nuclear detonation. Such a pulse is appropriate for studying the effect of the

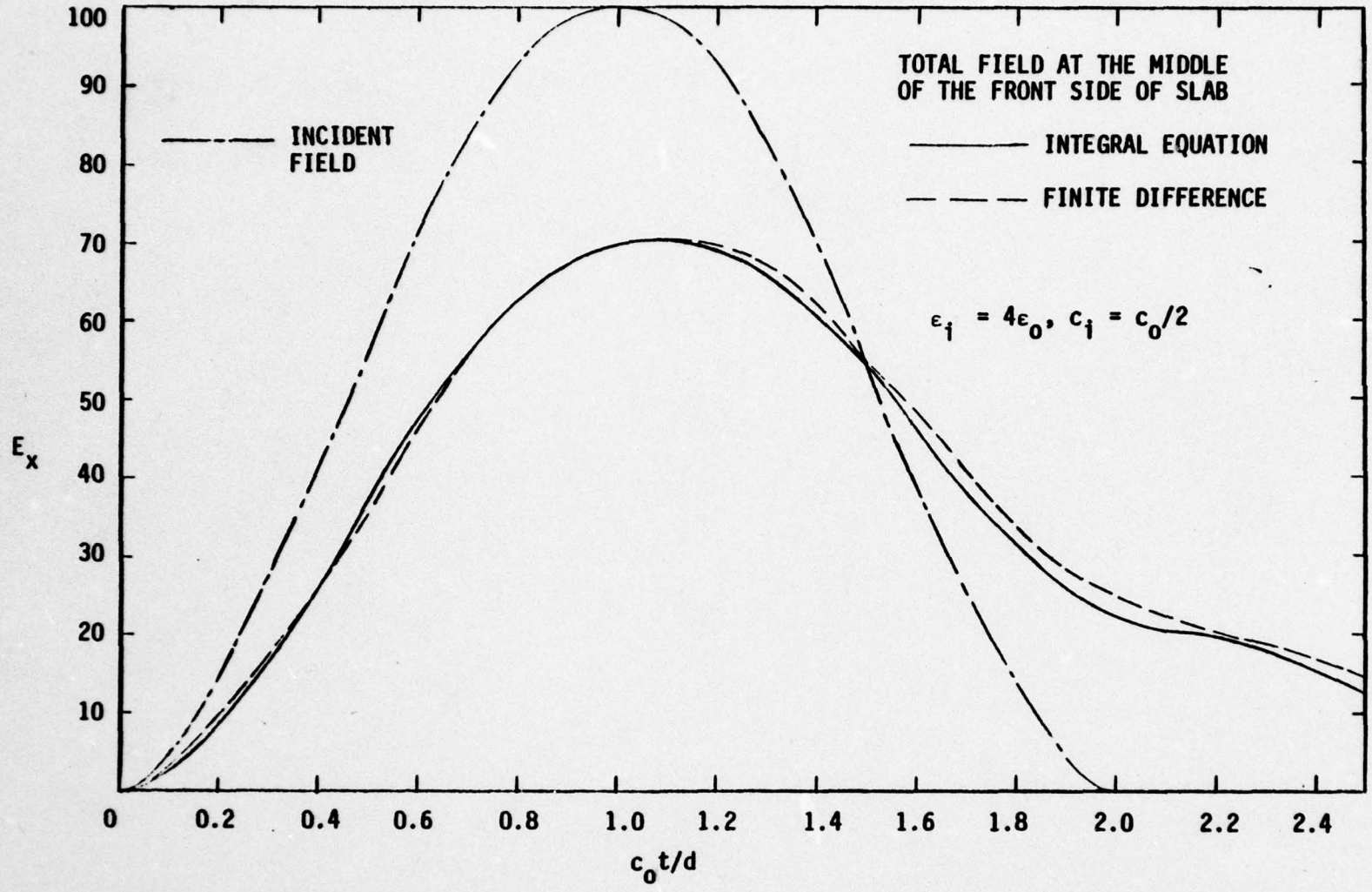

Figure 20. Comparison Between the Integral Equation and Finite Difference Methods for the Calculation of the Total Field at the Middle of the Front Side of the Slab. Units for Field Strength are Arbitrary

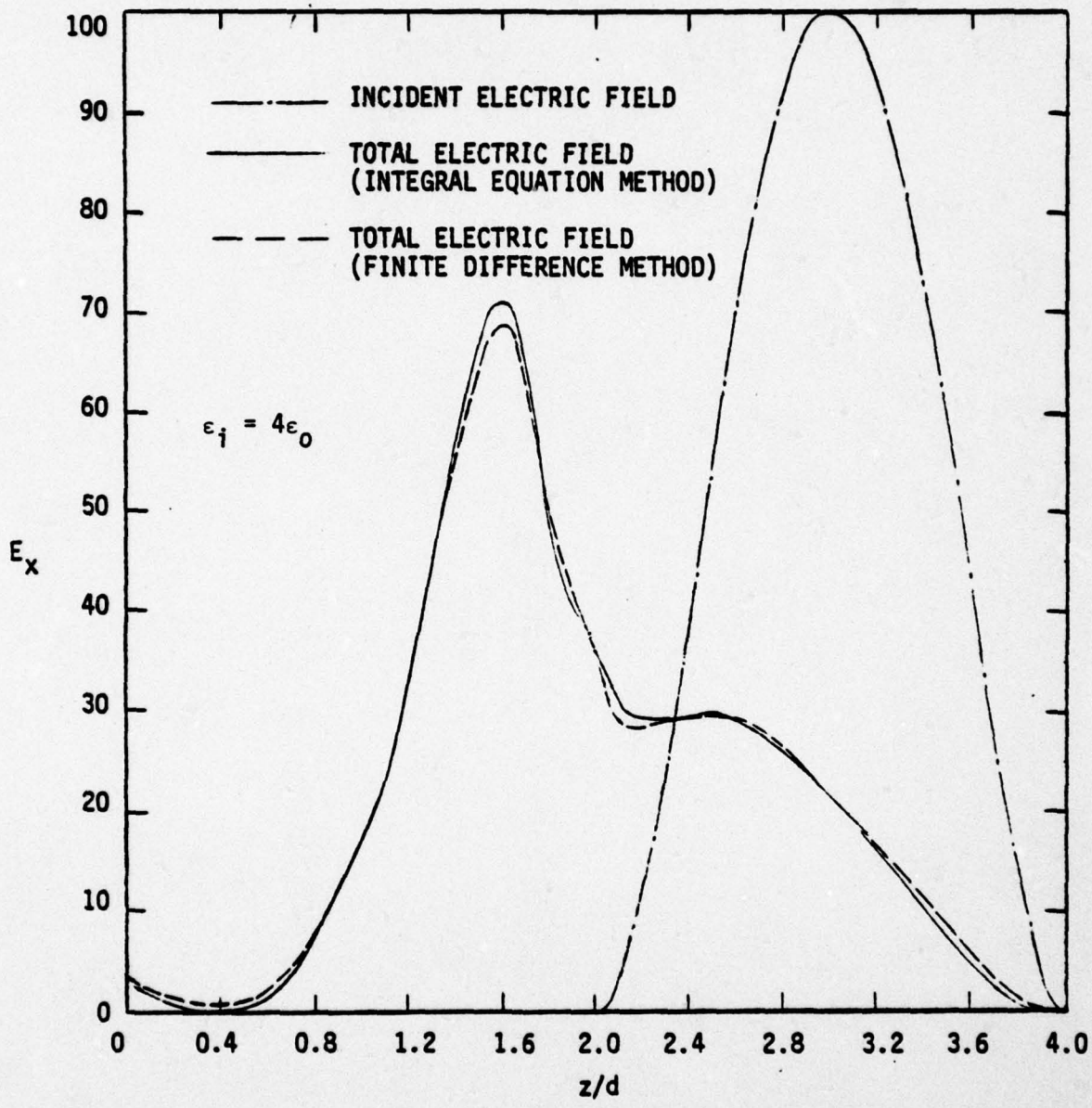

Figure 21. Comparison of Integral Equation and Finite Difference Methods for the Calculation of the Total Electric Field on the Top Side of the Slab (y = 0)

ATLAS I simulator trestle platform on the incident electromagnetic pulse. We will discuss the applicability of our results to the ATLAS I trestle platform problem later on in this section. The incident pulse is given by

$$E^{inc} = \psi^{inc} = 331361(d/c_o t)^3 \, e^{-121.5(d/c_o t)^2}. \qquad (39)$$

This pulse has a smooth wavefront (all derivatives vanish at $t = 0$) and it reaches a maximum of 101.422 (arbitrary units) at $c_o t = 9d$. However, at $c_o t = 3d$ the pulse has only risen to 0.017. For this reason we arbitrarily set $t = 0$ when the field strength at $z = 0$ is 0.017. Thus the effective rise time is $6d/c_o$, i.e., from 0.017 to peak. If we adopt the definitions given in references 4 and 5 then for our pulse $t_{max\ rise} \approx \psi^{inc}_{max}/(d\psi^{inc}/dt)_{max} \approx 3.03\ d/c_o$ and $t_{10\text{-}90}$ = 10% to 90% rise time $\approx$ 2.98 d/c_o. The reason we chose equation 39 for our incident pulse is that the usual double exponential employed by other workers to represent the true EMP has a discontinuous first derivative at $t = 0$. (Notice that we could also have employed the inverse double exponential waveform $\psi^{inc} = \psi_o[(\exp(-\alpha(t-t_o)) + \exp(\beta(t-t_o))]^{-1}$ (refs. 4 and 5) for which all derivatives at $t = 0$ exist. A suitable choice for t_o should make ψ^{inc} at $t = 0$ as small as desired.)

We have plotted the total electric field at points above the slab versus the distance from the origin, with the vertical distance from the top of the slab and the dielectric permittivity as parameters. It is assumed that the effective wavefront (i.e., a field strength of 0.017) hits the edge at $t = 0$. In figure 22 the graph for $z = 5d$ starts at $c_o t/d = 6$ and at this instant the

---

4. Baum, C. E., Some Considerations Concerning Analytic EMP Criteria Waveforms, Theoretical Note 285, Air Force Weapons Laboratory, October 1976.

5. Castillo, J. P., K. C. Chenand and C. E. Baum, Relation of Rise Time Definitions for Various Waveforms, Atlas Memo 20, Air Force Weapons Laboratory, November 1976.

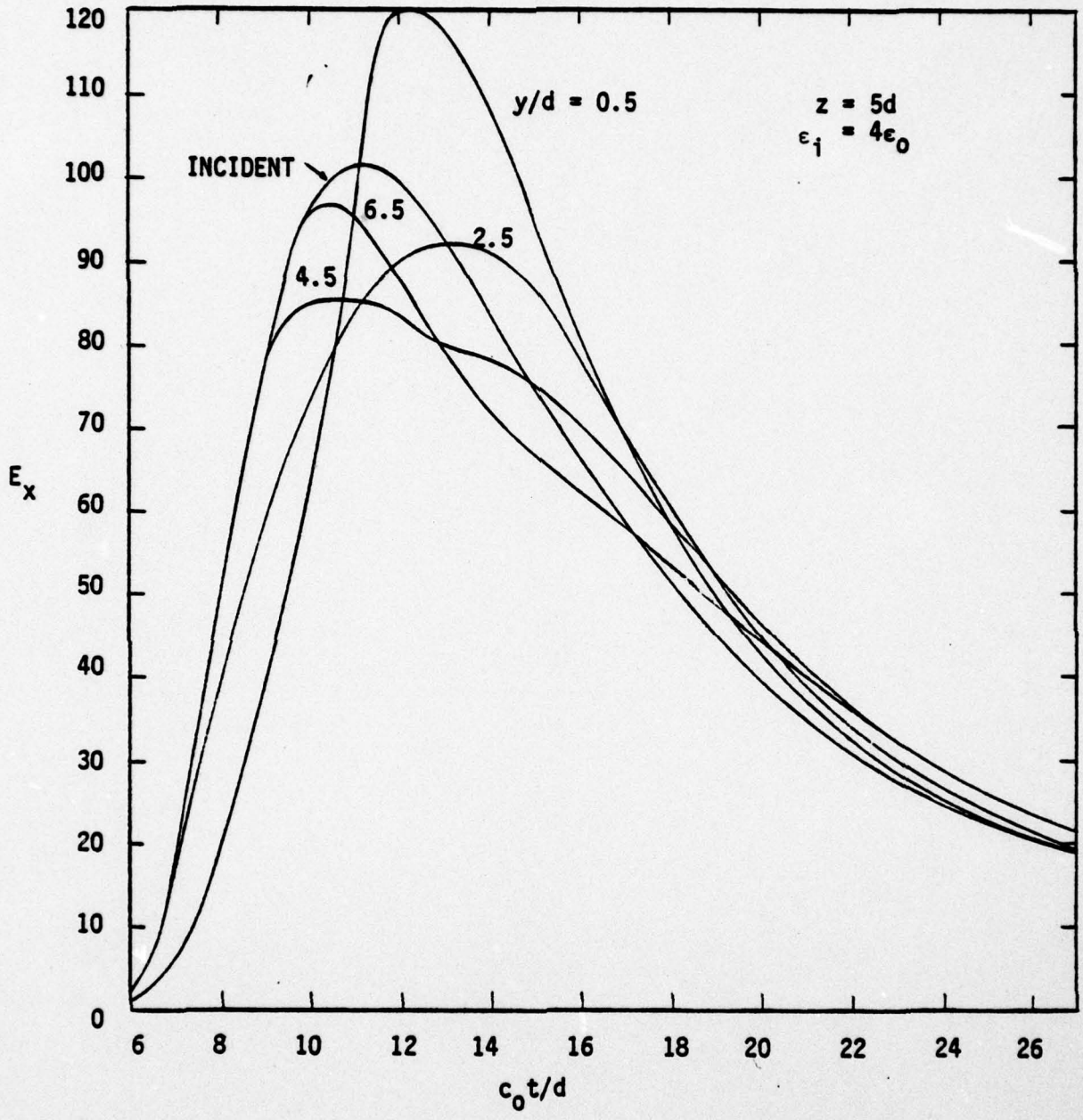

Figure 22. Incident and Total Electric Field (in Arbitrary Units) Versus Normalized Time at z = 5d with $\varepsilon_i = 4\varepsilon_o$. The Normalized Distance Above the Slab is the Parameter

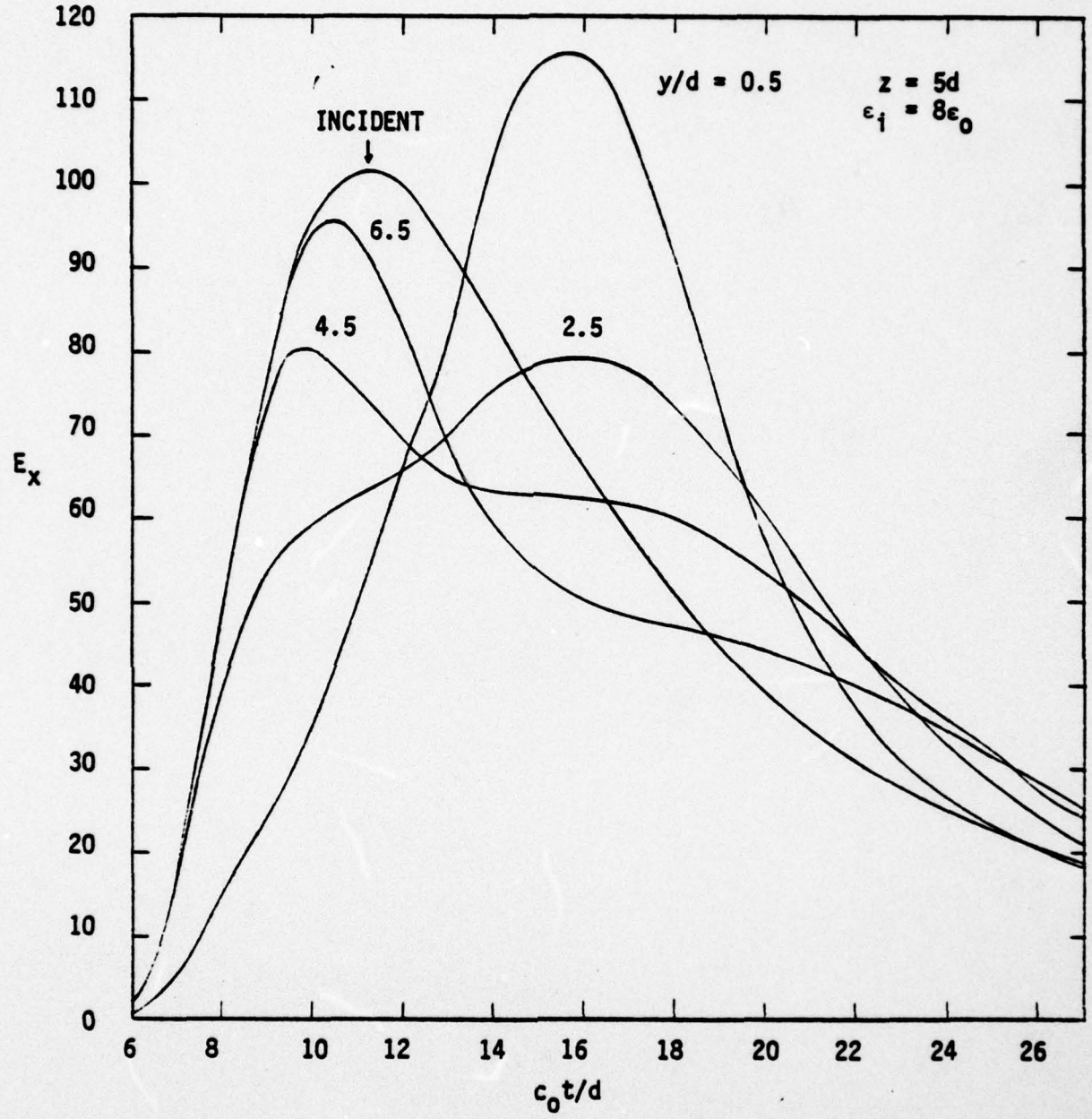

Figure 23. Incident and Total Electric Field (in Arbitrary Units) Versus Normalized Time at z = 5d with $\varepsilon_i = 8\varepsilon_o$. The Normalized Distance Above the Slab is the Parameter

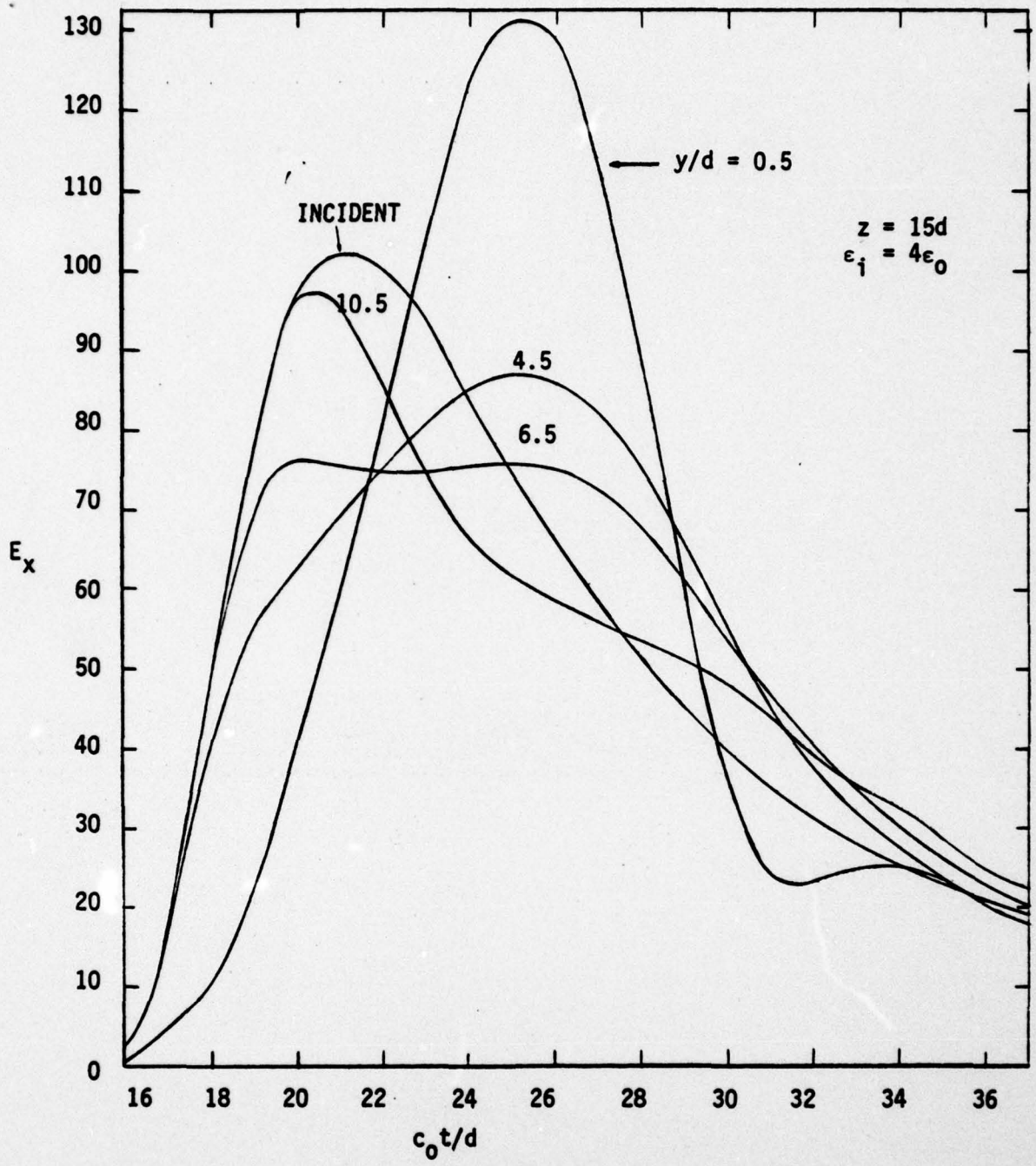

Figure 24. Incident and Total Electric Field (in Arbitrary Units) Versus Normalized Time at z = 15d with $\varepsilon_i = 4\varepsilon_o$. The Normalized Distance Above the Slab is the Parameter

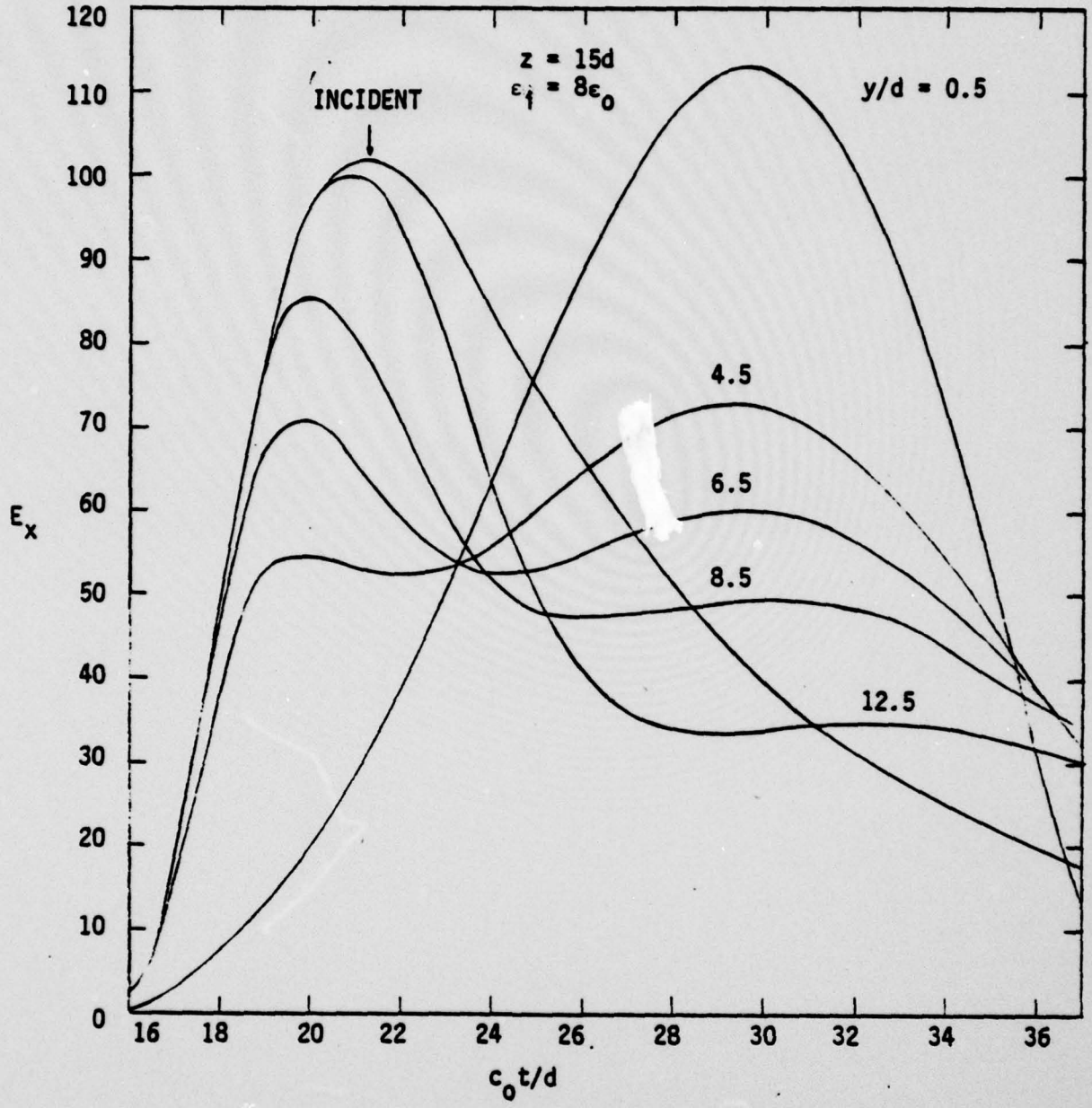

Figure 25. Incident and Total Electric Field (in Arbitrary Units) Versus Normalized Time at z = 15d with $\varepsilon_i = 8\varepsilon_o$. The Normalized Distance Above the Slab is the ^{o}Parameter

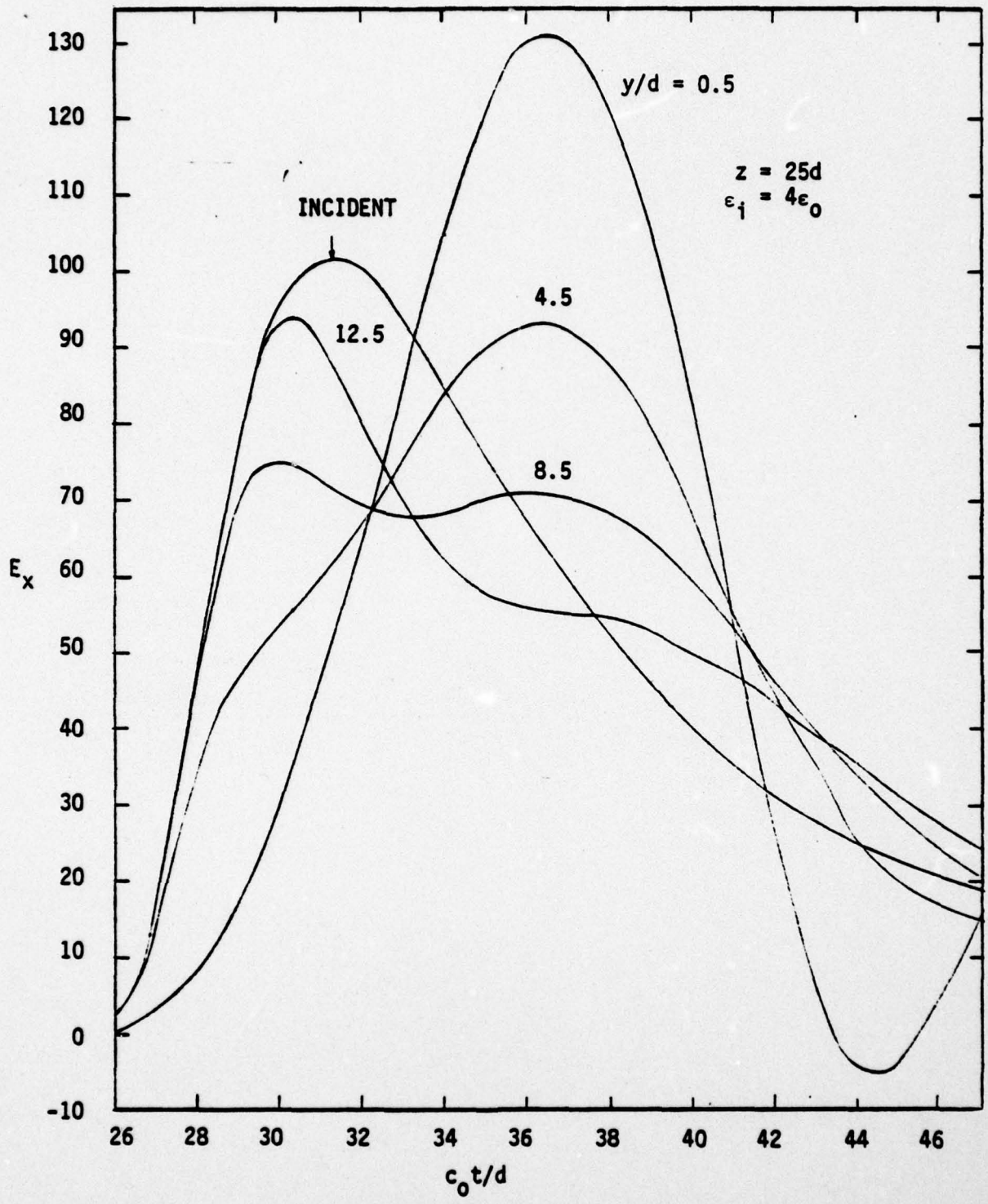

Figure 26. Incident and Total Electric Field (in Arbitrary Units) Versus Normalized Time at z = 25d with $\varepsilon_1 = 4\varepsilon_o$. The Normalized Distance Above the Slab is the Parameter

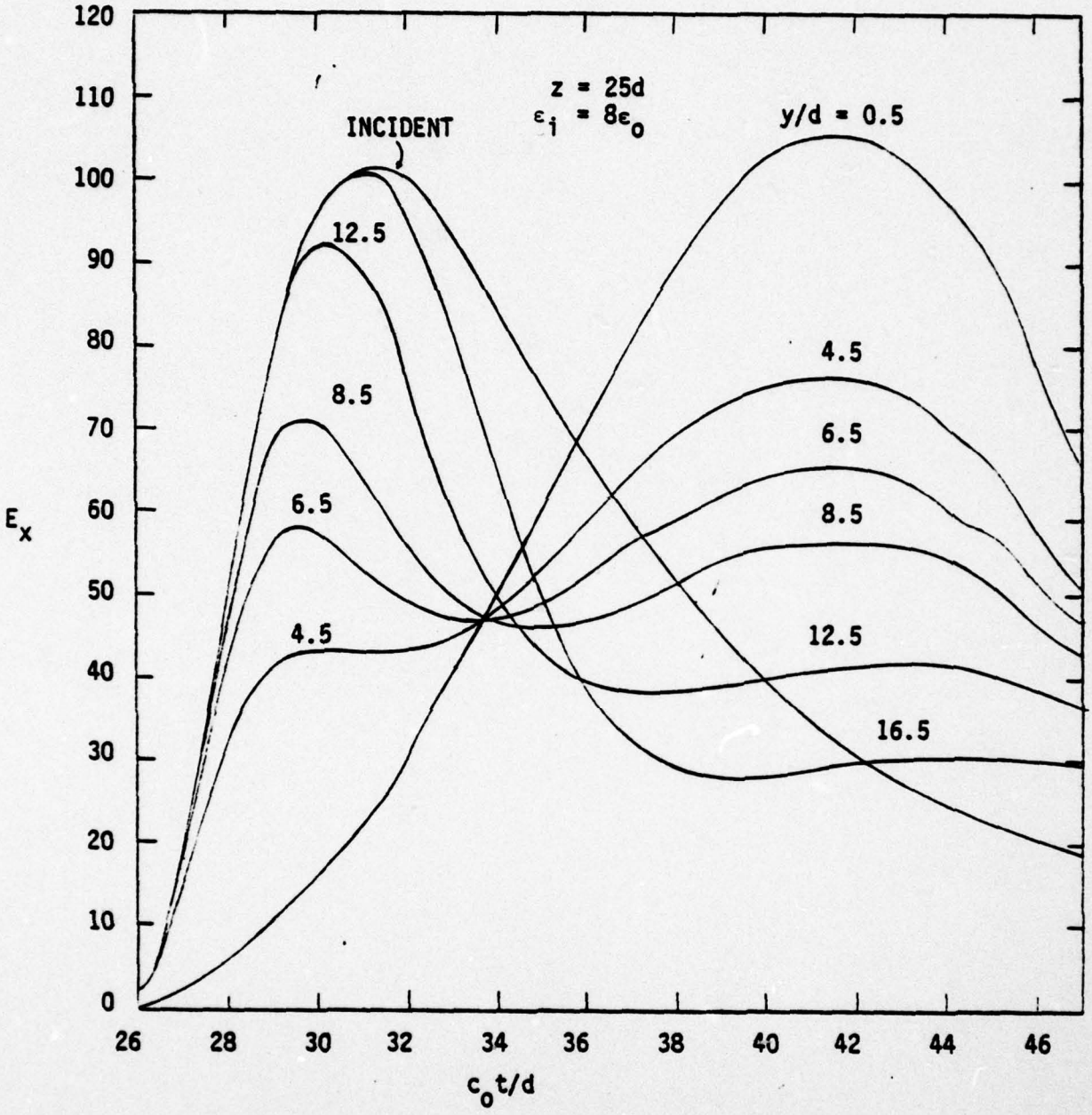

Figure 27. Incident and Total Electric Field (in Arbitrary Units) Versus Normalized Time at z = 25d with $\varepsilon_i = 8\varepsilon_o$. The Normalized Distance Above the Slab is the Parameter

incident field has a value of 2.6, i.e., the effective wavefront has already passed the point $z = 5d$ for a length of time $\Delta t = d/c_o$. Graphs at points further away from the edge also show the actual times corresponding to the incident wave sweeping by. Thus at $z = 15d$ we start at $t = 16d/c_o$ and at $z = 25d$ at $t = 26d/c_o$. To obtain the results displayed on the graph through $z = 25d$ we pushed the memory requirements under CDC 7600 FTN4 to the limit and therefore we were forced to use a relatively coarse grid size, $h = d/7$. Thus we cannot guarantee the accuracy of the results. However, results for $h = d/21$ (at $z = 5d$) and $h = d/11$ (at $z = 15d$) were similar to those at $h = d/7$ over the common region in space and time, the maximum deviation being 1 to 2 percent of the peak incident field.

The plots show that the presence of the slab can distort the incident field significantly. On the top surface of the slab or very close to it, the total field reaches a maximum that is shifted in time relative to the maximum of the incident field. This maximum is also larger than the peak value of the incident field. The behavior of the total field can be qualitatively understood if we take into account the secondary wave within the slab propagating with a speed $c = c_i$. The larger the dielectric permittivity the slower the secondary wave is (i.e., smaller c_i) and the total field reaches its peak later. This can be seen from the graphs for $\varepsilon_i = 4\varepsilon_o$ and $\varepsilon_i = 8\varepsilon_o$. As the observation point moves upward the total field tends to exhibit two humps until it is sufficiently high where, due to the diminishing influence of the slab, resembles the incident field. As the observation point rescinds from the edge the presence of the slab becomes more pronounced and one must reach progressively higher observation points (larger y/d) before the influence of the slab has diminished. Thus at $z = 5d$, $y = 6.5d$ ($\varepsilon_i = 8\varepsilon_o$) the field exhibits, in some approximate manner, the same distortion as the field at $z = 25d$, $y = 16.5d$ ($\varepsilon_i = 8\varepsilon_o$).

1. THE ATLAS I TRESTLE PLATFORM

Our two-dimensional scattering from a rectangular dielectric slab can serve as a model for studying the influence of the wood support structure (trestle), of the ATLAS I simulator, on the waveform of the simulated EMP. We will only focus our attention on the platform, i.e., ignore the rest of the support structure. (See references 6 and 7 for a study of the reflection of a plane wave from the rest of the support structure.) This platform is depicted in figure 28. First notice that the effective rise time of the incident pulse given by equation 39 is 6d and since the platform thickness is approximately 2 feet this effective rise time is translated into 12 nsec. Whereas $t_{\text{max rise}}$ and $t_{10\text{-}90}$ are approximately equal to 6 nsec. Thus our pulse is faster rising (also faster decaying) than the actual pulse to be fired in the ATLAS I simulator (see ref. 8 for the waveforms obtained in the pulser test fixture (PTF) with the ATLAS prototype pulser module and ref. 9 for a summary of the final results of all testing performed on the ATLAS prototype pulser module in PTF and also the influence of additional diffraction and relfection effects on the waveform of the pulse.) This difference in the rise time and other pulse characteristics between our pulse and the one to be fired into the working volume of ATLAS I makes our quantitative results

---

6. Prather, W. D., The Reflection of Electromagnetic Waves from an Array of Electrically Small Metal Bolts and Rings, ATLAS Memo 15, Air Force Weapons Laboratory, September 1974.
7. Prather, W. D., Lt. J. Little, Maj. R. Blackburn and K. Chen, The Reflection of Electromagnetic Waves from a Wooden Test Stand, ATLAS Memo 16, Air Force Weapons Laboratory, November 1974.
8. Maxwell Laboratories, Inc., TRESTLE Prototype Pulser Test Report, Volumes I and II, Report MLR-483, November 1975.

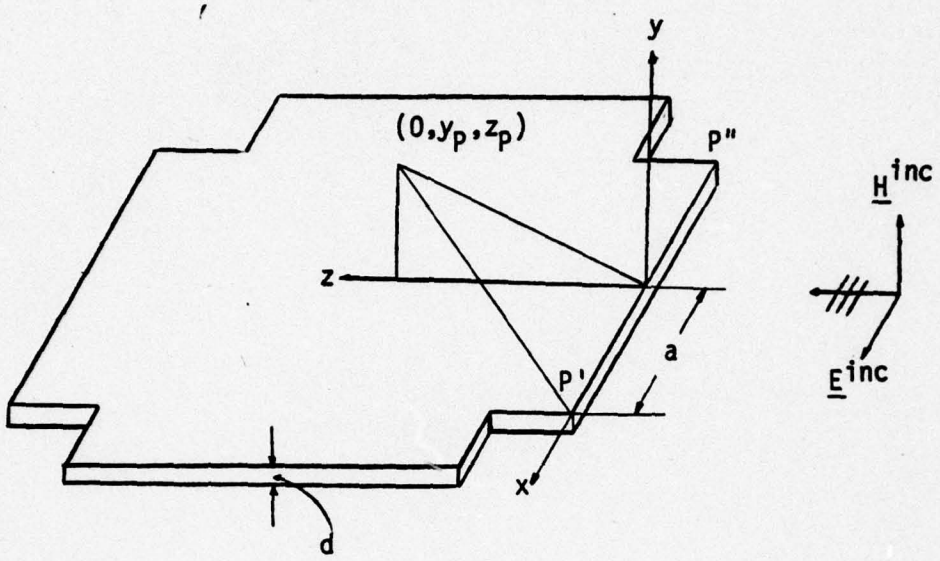

Figure 28. Geometry of the ATLAS I Trestle Platform for the Calculation of "Clear" Time Interval

not directly applicable; our results, however, can still provide information on the influence of the platform on the waveform of a fast rising and slowly decaying pulse. Next we observe that our two-dimensional study is valid as long as it is applied to observation points that have not been reached by the diffracted waves due to the edges P', P". Choosing our observation points on the x = 0 plane the maximum or clear time interval over which our two-dimensional model is valid is the time that elapses from the instant the incident field reaches the observation point P until the instant the diffracted fields from edges P', P" reach P (fig. 28), i.e.,

$$c_o T_{max}/d = \left[\left(a^2 + z_P^2 + y_P^2\right)^{1/2} - \left(z_P^2 + y_P^2\right)^{1/2}\right]/d$$

For the trestle platform $a \approx 70'$, $d \approx 2'$. Thus

$c_o T_{max}/d$	z_P/d	y_P/d
30	5	0.5
28	5	6.5
23	15	0.5
21	15	10.5
18	25	0.5
16	25	16.5

Thus, assuming that $\varepsilon_i = 4\varepsilon_o$ for the wood platform, $c_o t/d$ in figure 22 extends throughout the indicated region, in figure 24 approximately throughout the indicated region and in figure 26 up to an average of 26 + 17 = 43. In any case the graphs show the distortion of the incident waveform due to the presence of the platform, over a large portion of the incident pulse, well past its rise time.

---

9. Baum, C. E., D. E. Higgins and D. V. Giri, Pulser Test Results and Preliminary Estimation of Transient Electric Field Waveforms in ATLAS I, ATLAS Memo 18, Air Force Weapons Laboratory, Oct. 1976.

SECTION VI

COMPARISON OF THE INTEGRAL EQUATION AND FINITE DIFFERENCE METHODS

In this section a comparison is drawn between the integral equation method and the finite difference scheme based on the required computational resources and degree of overall simplicity.

1. MEMORY REQUIREMENTS

a. Finite Difference Scheme

In order to ensure that the imposed boundary conditions discussed in section IV do not affect the accuracy of the field strengths computed in the region outside the dielectric body, it is necessary that the grid extend a distance c_oT in the positive and negative z-directions and in the distance above the platform, where T is the length of the time from when the incident field first hit the body until the latest time of interest. (Due to symmetry about the plane $y = y_m < 0$, where y_m is the y coordinate of the middle of the front side, only the $y > y_m$ region need be considered.) If the only fields of interest are those on or inside the body, the grid need only be extended to a distance $c_oT/2$ instead of c_oT. (This can be understood by recalling the influence of the boundary conditions discussed in section IV.) Thus the grid size must be $2c_oT(c_oT + d/2)/h^2$ in the former case and $c_oT(c_oT/2 + d/2)/h^2$ in the latter case where h is the grid step size. The finite difference algorithm requires knowledge of the fields at the present time step and the previous time step in order to compute the fields at the next time step. However, the field strength at a given grid point at the previous time step is only needed to compute the value at the next time step at the same grid point and consequently it is only necessary to provide two storage locations for each grid point.

b. Integral Equation Method

The integral equation method permits a tradeoff in costs. Instead of recomputing the influence coefficients, discussed in section III, for each time step, it is possible to store them for future use and compute only those coefficients relating the present time step to the first time step. We can do this because the kernel of the integrals defining the influence coefficients depends on t - t' and not t or t' individually. Thus there is a tradeoff in that presumably memory references are faster than evaluation of transcendental functions (resulting from the explicit calculation of the double integrals defining the influence coefficients) and the logic required to determine whether or not a zone can influence the reference point. Under the assumption that this tradeoff of memory for computer time will be used, $4N^2(T/\Delta t)$ memory location are required to store the influence coefficients where N is the number of line segments and Δt is the time step size. This number of memory locations can be reduced by implementing existing symmetry relations (e.g., interaction of neighboring line segments is independent of location provided that the segments lie on the same side) but the basic dependence remains unchanged. It should be noted here that, for the angle of incidence of the incident field we are considering in this report, if the length of the top and bottom sides of the rectangle is greater than c_oT, N can be reduced to ignore the region of the rectangle that will not be illuminated by the incident field by time c_oT. Thus for such cases the number of memory locations for the influence coefficients depends on three additive terms proportional to T, T^2 and T^3 respectively, and if the front side is much smaller than c_oT, T^3 dominates. In addition the integral equation method requires knowledge of $\dot{\Psi}$ and Φ for all previous times, i.e., $2N(T/\Delta t)$ memory locations whether or not the influence coefficients are stored.

2. COMPUTATION TIME

a. Finite Difference Scheme

Ignoring the boundary points which require special treatment each grid point requires the same length of time at each step. From the form of the difference scheme which replaces the differential equation at each grid point we can see that three multiplications, six additions and eight array references are needed for the calculation of the field strength at given grid point at the next time step. These operations must be performed for each grid point for each time step, i.e., $c_o T^2 (c_o T + d/2) T_1^*/h^2$ overall computation time is required over the time of interest T, where T_1^* is the time length of the operations indicated above. If $c_o T >> d/2$ the time required is proportional to T^3. This result may be reduced by factor of three by recognizing that in calculating the field strength at a grid point at t the finite difference technique need not be applied to points at a distance greater than $c_o t$ from the body because the scattered field has only traveled a distance $c_o t$ and the field strength at grid points outside this region is that of the incident field. If the total period of interest is T then the computation time is approximately $c_o^2 T^3 T^*/3h^2$ if $c_o T >> d/2$. (The factor of three comes from $\int_o^T t^2 dt = T^3/3$.)

b. Integral Equation Method

As we explained in our discussion of the computation time for the finite difference scheme each grid point requires the same length of time at each time step independently of the parameters of the system, i.e., length of time the body has been exposed to the incident field, size of body and step size. Unlike the finite difference scheme the central processor time for the integral equation method depends on all those parameters. Assuming now that the influence

coefficients have already been calculated and stored the calculation of the fields at time t requires approximately $4N^2(t/\Delta t)$ multiplcations and additions. Thus to extend the calculation to time T requires $2N^2(T/\Delta t)^2$ multiplications and additions, and if T_2^* is the time of one multiplication plus one addition the computation time is $2N^2(T/\Delta t)^2 T_2^*$. The calculation of the influence coefficients requires the calculation of $4N^2(T/\Delta t)$ double integrals. Even though for our geometry these integrals can be done analytically, the necessary evaluation of the resulting transcendental functions will contribute a significant amount to $2N^2(T/\Delta t)^2 T_2^*$ unless $T/\Delta t$ is large. It should be noted that the above discussion assumed that only the surface fields were of interest. For points off the surface of the body the calculation of Ψ at a given time t requires $2N(t - R/c)/\Delta t$ additional memory locations for the influence coefficients and $2N(t - R/c)/\Delta t$ additional multiplications and additions where R the average distance of the reference points on the surface of the body to the observation point off the surface. (If Ψ at the same point is desired for a series of equally spaced time steps, the required number of integral evaluations will depend only on the greatest time of interest, not on the number of values wanted.)

3. CONCLUSIONS

As we mentioned in the beginning of this section the comparison between the two methods will be based on the degree of overall simplicity and the required computational resources. With respect to deriving the necessary equations and casting them into a form suitable for numerical calculation the finite difference scheme is much simpler than the integral equation method and this simplicity is definitely a great advantage. Both methods can be made comparable in accuracy but the required computational resources for

the two methods depend differently on the length of time of interest and this factor influences the regions over which one method can be superior to the other. To understand this point recall that the finite difference method requires approximately $4c_o^2T^2/h^2$ memory locations and $c_o^2T^3T_1^*/3h^2$ compuatation time whereas the integral equation method requires approximately $4N^2(T/\Delta t)$ (or $T^3/(\Delta t)^3$ if the incident wave has illuminated a length c_oT of the body and $c_oT >> d/2$) memory locations and $2N^2(T/\Delta t)^2T_2^*$ computation time. Thus assuming that $2c_o\Delta t \approx h$ we understand that when $T/\Delta t < N^2$ the finite difference scheme is preferable. However, for large times, i.e., $T/\Delta t > N^2$ the integral equation method requires fewer computational resources and should be considered if the simplicity of the difference equation scheme is overridden by an appreciably smaller cost for the integral equation method. If the field strength must be calculated at points far away from the body, the integral equation method is more practical since the finite difference scheme requires propagating the field from the body to the region of interest whereas for the integral equation method the distance from the body has no effect on the required resources.

Our conclusions about computer resources were based on the two-dimensional model of the wave equation. For a three-dimensional model the finite difference method would again be relatively insensitive to the dimensions of the body. Memory requirements would vary as T^3 hence total time will vary as T^4. For the integral equation method it is no longer necessary to store influence coefficients and field strengths for all time but only for $r_m/c_i\Delta t$ time steps where r_m is the maximum diameter of the body. The number of patches will vary as L^2/h^2 where L and h are characteristic dimensions of the body and spatial step size,

hence the matrix of influence coefficients requires of the order of $(L^2/h^2)^2(r_m/c_i\Delta t)$ memory locations. Similarly the number of field strengths required is $(L^2/h^2)(r_m/c_i\Delta t)$. The time per patch per step varies as $(L^2/h^2)(r_m/c_i\Delta t)$ hence total time varies as $(L^2/h^2)(r_m/c_i\Delta t)T$. From the above brief discussion we understand that we can draw similar conclusions about the relative merits of the two methods as for the two-dimensional comparison.

APPENDIX A

REFLECTION FROM A DIELECTRIC HALF SPACE

We assume that the incident electric field has the form $\underline{E}^{inc} = \Psi^{inc}\,\hat{e}_x$ where $\Psi^{inc} = f(t - y_1/c_o) = f[t - 1/c_o(y \sin\alpha - z\cos\alpha)]$ (fig. A1). Thus at the boundary surface ($z = 0$) $\Psi^{inc} = f(t - y/c_o \sin\alpha)$. It is reasonable to assume that the total surface field Ψ and $\partial\Psi/\partial n'$ will only depend on $t - y/c_o \sin\alpha$, i.e., as the incident surface field propagates to the right the total surface field keeps pace with it. By noting that $(\underline{\rho}' - \underline{\rho}) \cdot \hat{n} = (y' - \underline{y})\hat{e}_y \cdot \hat{e}_z = 0$, equations 17 can be written as follows

$$\frac{1}{2}\Psi(o,t) = \Psi^{inc} - \frac{c_o}{2\pi}\int_{-\infty}^{\infty}\int_{-\infty}^{\infty}\frac{U\left[c_o(t-t') - |y'|\right]}{\left[c_o^2(t-t')^2 - y'^2\right]^{1/2}}\frac{\partial\Psi}{\partial n}\,dy'dt'$$

$$\frac{1}{2}\Psi(o,t) = \frac{c_i}{2}\int_{-\infty}^{\infty}\int_{-\infty}^{\infty}\frac{U\left[c_i(t-t') - |y'|\right]}{\left[c_i^2(t-t')^2 - y'^2\right]^{1/2}}\frac{\partial\Psi}{\partial n}\,dy'dt' \qquad \text{(A-1)}$$

Invoking causality we understand that the upper limit of the t' integration can be replaced by t. (The lower limit is of no interest for the calculation in this appendix.) Setting $U = 1$ we obtain $y' = \pm c(t - t')$ as the limits of the y' integration.

Next we set $t - t' = \tau$ and the limits of the τ and y' integrations are (o,∞) and $(-c\tau, c\tau)$ respectively. Recalling that $\partial\Psi/\partial n$ only depends on $t' - (y'/c_o)\sin\alpha$ we make the following orthogonal transformation

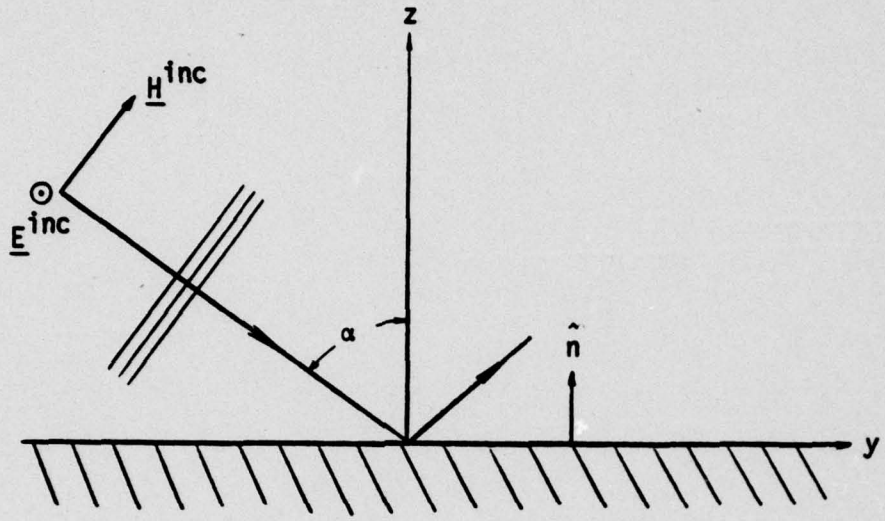

Figure A1. Geometry Depicting the Oblique Incidence of an Electromagnetic Pulse onto an Infinite Dielectric Half Space

$$u = \tau + \frac{y'}{c_o} \sin \alpha$$

$$v = -\tau \sin \alpha + \frac{y'}{c_o} . \qquad \text{(A-2)}$$

Thus $\partial\Psi/\partial n$ is a function of $t' - (y'/c_o) \sin \alpha = t - \tau - (y'/c_o) \sin \alpha$, i.e., a function of $t - u$ which is independent of v since t is just a constant. This will allow us to do the v-integration explicitly. Noting that $dudv = 1/c_o(1 + \sin^2 \alpha)\, d\tau dy'$ and referring to figure A2 we can rewrite equations A-1 as

$$\frac{1}{2} \Psi(o,t) = \Psi^{inc}(o,t) - \frac{1}{2\pi} \int_o^\infty \frac{\partial \Psi}{\partial n}\, du \int_{L_1^- u}^{L_1^+ u} \frac{dv}{\left(A_1 v^2 + B_1 v + C_1\right)^{1/2}}$$

$$\frac{1}{2} \Psi(o,t) = \frac{\gamma}{2\pi} \int_o^\infty \frac{\partial \Psi}{\partial n}\, du \int_{L_2^- u}^{L_2^+ u} \frac{dv}{\left(A_2 v^2 + B_2 v + C_2\right)^{1/2}} \qquad \text{(A-3)}$$

where $L_1^{\pm} = \dfrac{1 \mp \sin \alpha}{\sin \alpha \pm 1}$

$$L_2^{\pm} = \frac{\gamma \mp \sin \alpha}{\gamma \sin \alpha \pm 1} , \quad \gamma = \frac{c_i}{c_o}$$

$$A_1 = -\cos^2 \alpha \qquad A_2 = \gamma^2 \sin^2 \alpha - 1$$

$$B_1 = -4 \sin \alpha \qquad B_2 = -2(1 + \gamma^2) \sin \alpha$$

$$C_1 = \cos^2 \alpha \qquad C_2 = \gamma^2 - \sin^2 \alpha .$$

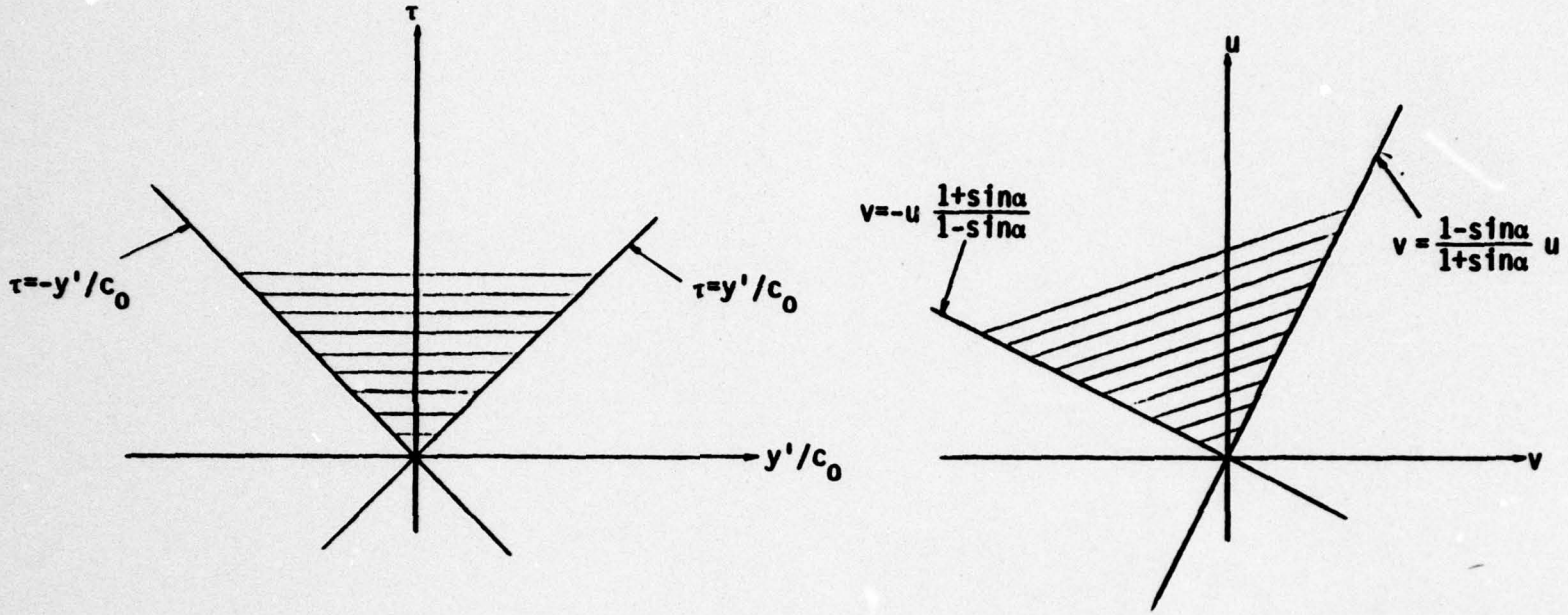

Figure A2. Coordinate Transformation Relevant to the Evaluation of an Integral in Appendix A

If we perform the v-integration we obtain

$$\frac{1}{2}\Psi(o,t) = \Psi^{inc}(o,t) - \frac{1}{2\cos\alpha} I$$

$$\frac{1}{2}\Psi(o,t) = \frac{\gamma}{2}\frac{1}{\left(1-\gamma^2\sin^2\alpha\right)^{1/2}} I \qquad \text{(A-4)}$$

where $I = \int_o^\infty \frac{\partial\Psi}{\partial n}\, du.$

Solving Equation A-4 for $\Psi(o,t)$ we obtain

$$\frac{\Psi(o,t)}{\Psi^{inc}(o,t)} = \frac{2\gamma\cos\alpha}{\gamma\cos\alpha + \left(1-\gamma^2\sin^2\alpha\right)^{1/2}}, \quad \gamma = \frac{c_i}{c_o} \qquad \text{(A-5)}$$

i.e., the well-known result for the transmission coefficient.

APPENDIX B

REFLECTION FROM A DIELECTRIC SLAB

To simplify our calculation we will assume broadside incidence, i.e., $\underline{E}^{inc} = \Psi^{inc}\,\hat{e}_x = f(t + z/c_o)\hat{e}_x$ (fig. B1). In appendix A the $\partial\Psi/\partial t$ term in equations 17 was not considered because $(\underline{\rho}' - \underline{\rho}) \cdot \hat{n}' = 0$ for the surface of an infinite half space. In the present case $\underline{\rho}'$ and $\underline{\rho}$ can belong to different surfaces and $(\underline{\rho}' - \underline{\rho}) \cdot \hat{n}'$ is not necessarily zero. Thus in this appendix we will check the validity of equations 17 when both $\partial\Psi/\partial t$ and $\partial\Psi/\partial n$ are retained whereas in appendix A only $\partial\Psi/\partial n$ was retained.

Due to the broadside incidence Ψ, $\partial\Psi/\partial t$ and $\partial\Psi/\partial n$ are independent of y. Thus the y'-integration can be performed explicitly by setting U = 1 and determining the limits of the t',y' integrations and equations 17 reduce to

$$\frac{1}{2}\,\Psi(t,z=0) = \Psi^{inc}(t,z=0) - \frac{c_o}{2}\int_{-\infty}^{t} \left.\frac{\partial\Psi}{\partial n}\right|_{z=0} dt' - \frac{c_o}{2}\int_{-\infty}^{t-d/c_o} \left.\frac{\partial\Psi}{\partial n}\right|_{z=-d} dt'$$

$$- \frac{1}{2}\,\Psi(t - d/c_o,\ z = -d)$$

$$\frac{1}{2}\,\Psi(t,z=0) = \frac{c_i}{2}\int_{-\infty}^{t} \left.\frac{\partial\Psi}{\partial n}\right|_{z=0} dt' + \frac{c_i}{2}\int_{-\infty}^{t-d/c_i} \left.\frac{\partial\Psi}{\partial n}\right|_{z=-d} dt'$$

$$+ \frac{1}{2}\,\Psi(t - d/c_i,\ z = -d)$$

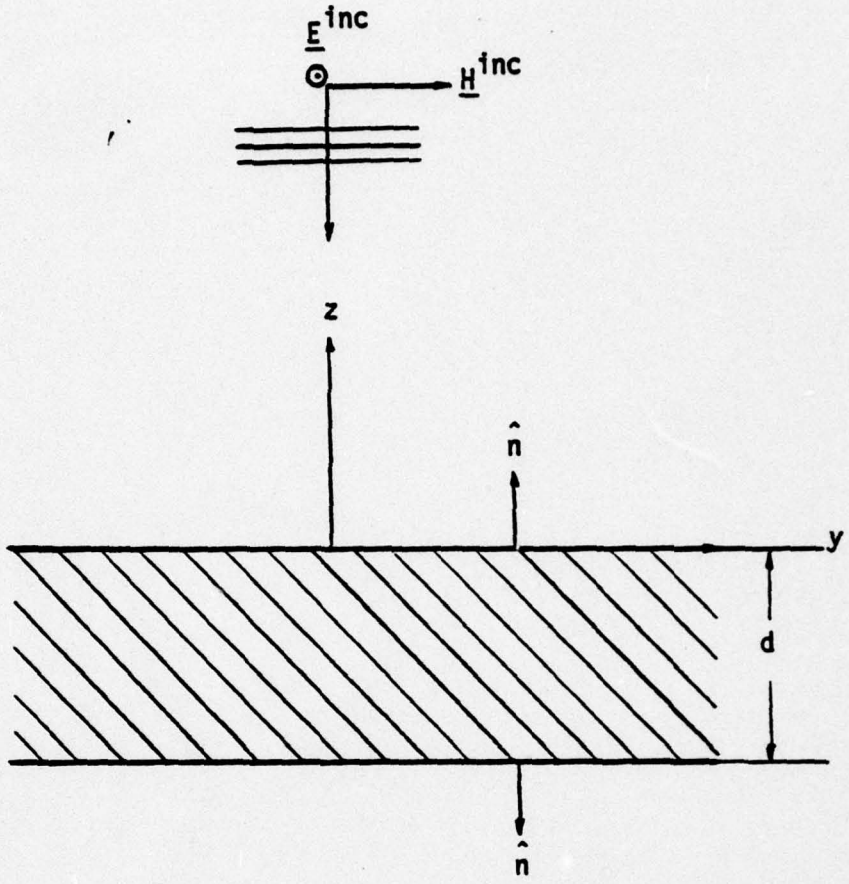

Figure B1. Normal Incidence of an Electromagnetic Pulse Onto an Infinite Dielectric Slab of Thickness d

$$\frac{1}{2}\,\Psi(t,z=-d) = \Psi^{inc}(t,z=-d) - \frac{c_o}{2}\int_{-\infty}^{t-d/c_o} \left.\frac{\partial\Psi}{\partial n}\right|_{z=0} dt' - \frac{c_o}{2}\int_{-\infty}^{t} \left.\frac{\partial\Psi}{\partial n}\right|_{z=-d} dt'$$

$$- \frac{1}{2}\,\Psi(t - d/c_o,\ z = 0)$$

$$\frac{1}{2}\,\Psi(t,z=-d) = \frac{c_i}{2}\int_{-\infty}^{t-d/c_i} \left.\frac{\partial\Psi}{\partial n}\right|_{z=0} dt' + \frac{c_i}{2}\int_{-\infty}^{t} \left.\frac{\partial\Psi}{\partial n}\right|_{z=-d} dt'$$

$$+ \frac{1}{2}\,\Psi(t - d/c_i,\ z = 0) \qquad \text{(B-1)}$$

Next we set

$$A(t) = \Psi(z = o,t), \qquad B(t) = \int_o^t \left.\partial\Psi/\partial n\right|_{z=0} dt'$$

$$C(t) = \Psi(z = -d,t), \qquad D(t) = \int_o^t \left.\partial\Psi/\partial n\right|_{z=-d} dt'$$

and equations B-1 can be rewritten as

$$A(t) = 2f(t) - c_oB(t) - c_oD(t - d/c_o) - C(t - d/c_o)$$

$$A(t) = c_iB(t) + c_iD(t - d/c_i) + C(t - d/c_i)$$

$$C(t) = 2f(t - d/c_o) - c_oB(t - d/c_o) - c_oD(t) - A(t - d/c_o)$$

$$C(t) = c_iB(t - d/c_i) + c_iD(t) + A(t - d/c_i) \qquad \text{(B-2)}$$

AD-A050 969 TDR INC LOS ANGELES CA F/G 20/14
NUMERICAL INVESTIGATION OF PLANE WAVE PULSE SCATTERING BY DIELE--ETC(U)
OCT 77 A D VARVATSIS, S G SIEGEL, M I SANCER AFOSR-76-3010
UNCLASSIFIED AFOSR-TR-78-0209 NL

2 OF 2
ADA
050969

END
DATE
FILMED
4-78
DDC

In order to solve Equations B-2 we transform them into the frequency domain:

$$A(\omega) + B(\omega) + C(\omega)\, e^{ik_o d} - D(\omega)\, e^{ik_o d} = 2f(\omega)$$

$$A(\omega) - c_i B(\omega) - C(\omega)\, e^{ik_i d} + c_i D(\omega)\, e^{ik_i d} = 0$$

$$A(\omega)\, e^{ik_o d} + c_o B(\omega)\, e^{ik_o d} + C(\omega) - c_o D(\omega) = 2f(\omega)\, e^{ik_o d}$$

$$-A(\omega)\, e^{ik_i d} - c_i B(\omega)\, e^{ik_i d} + C(\omega) + c_i D(\omega) = 0 \qquad \text{(B-3)}$$

Solving Equations B-3 for $A(\omega)$ we obtain the well-known result for the reflection coefficient $R(\omega)$

$$R(\omega) = A(\omega) - f(\omega) = \frac{(1 - \gamma^2)\, i \sin \alpha}{2\gamma \cos \alpha - i(1 + \gamma^2) \sin \alpha}$$

where $\gamma = c_i/c_o = k_o/k_i$.